



Oslo Metropolitan University
Faculty of Technology, Art and Design Department
of Mechanical, Electronic and Chemical Engineering

Accessibility
OPEN

BACHELORPROJECT

BACHELORPROJECTS TITLE Measurements of physical forces in cancer cells	DATE 25.05.2022
	NUMBER OF PAGES/ATTACHEMENTS 39/16
AUTHORS Emma Lillebø Thu Linda Mong Vu	INTERN SUPERVISOR Viola Lobert

IN COLLABORATION WITH Oslo University Hospital	EXTERNAL SUPERVISORS Anna Lång Stig Ove Bøe
---	---

SUMMARY <p>A broader knowledge on how cancer cells behave physically is important for understanding how they spread throughout the body. In order to understand how metastasis of cancer cells really works, it is necessary to know what happens with physical forces when cancer cells are awakened from quiescence.</p> <p>Cancer cells, isolated from three patients with urinary bladder cancer, were analyzed with live cell imaging and traction force microscopy.</p> <p>The cancer cell lines showed common features when it comes to traction forces arising after exit from quiescence and activation of cell migration. However, different migration patterns, in terms of single-cell and collective migration, as well as different migration velocities were observed.</p>
--

3 KEYWORDS
Migration
Traction forces
Urinary bladder cancer cells

Acknowledgments

This bachelor project was conducted from January to May 2022 at Oslo University Hospital, Department of Microbiology and Oslo Metropolitan University (OsloMet), Department of Mechanical, Electronics and Chemical Engineering. The project was carried out with help of the research group led by Stig Ove Bøe.

We would like to thank our main supervisor within the research group, Anna Lång. Thank you for your guidance and support during this period. Your help has been essential for us, especially during the laboratory, data analysis, and writing of this thesis. Since we are only undergraduate students with limited knowledge, you patiently explained and guided us through everything. This really contributed to our understanding and made writing on this thesis more manageable. Our stay and given experience would not have been the same without your enthusiasm and engagement.

We would like to express our gratitude to the research group, and for the opportunity to be a part of it. We appreciate Stig Ove Bøe's valuable opinions and perceptions which we used in this project and the explanation of Python-based scripts, and the teaching of standard tissue culture techniques. We would like to thank Emma Lång for always being available for questions and for the help with data analysis. Additionally, we want to thank Pernille Blicher for teaching us how to make polyacrylamide gels, as well as for performing experiments for us when we were unavailable.

We also want to show our appreciation to our supervisor at OsloMet, Viola Lobert, for being available for questions and helpful feedback, including your support throughout this project.

In addition, we would like to give an extra thanks to the security guard for always greeting us, both on the way in and home. Your uplifting smile made us feel welcome and encouraged our hectic days. Moreover, we are grateful to our families for their encouragement and moral support during this period.

Oslo, May 2022



Emma Lillebø



Thu Linda Mong Vu

Table of contents

Acknowledgments	1
Abstract	4
Abbreviations	5
1 Introduction	6
1.1 Cell cycle	6
1.1.1 Quiescence	7
1.2 Cell migration.....	8
1.2.1 Collective migration (of keratinocytes).....	8
1.3 Cancer	9
1.4 Urinary bladder anatomy	10
1.5 Urinary bladder cancer	11
1.5.1 Stages of urinary bladder cancer	11
1.6 Fluorescence in Biological Research.....	12
1.7 Microscopy and cell imaging.....	13
1.7.1 Traction force microscopy.....	15
1.8 Aims of the thesis.....	16
2 Materials and methods	16
2.1 Cell culture	16
2.1.1 Cell lines and culture conditions	16
2.1.2 Cell cultivation and passaging	16
2.2 Live cell imaging of migration pattern	17
2.2.1 Collagen IV coating	17
2.2.2 Cell count estimation.....	18
2.2.3 Cell seeding in 96-well plate.....	18
2.2.4 Cell starvation and re-stimulation of cells	19
2.2.5 Live cell imaging microscopy.....	20
2.2.6 Image processing.....	20
2.2.7 PIV analysis	21
2.3 Traction forces in cell monolayers.....	21
2.3.1 Preparation of collagen IV-coated polyacrylamide gels	21
2.3.2 Cell seeding on polyacrylamide gels	22
2.3.3 Traction force microscopy (TFM).....	22
2.4 Visualization of cancer cells by immunofluorescence (IF) staining.....	23
2.4.1 Preparation and fixation of cells for IF staining	23
2.4.2 Protocol for IF staining	24
2.4.3 Confocal microscopy	25
3 Results	25
3.1 Cell migration pattern	25
3.1.1 Cell migration patterns of asynchronously growing cancer cells.....	25
3.1.2 Cell migration patterns of quiescent and re-stimulated cancer cells	26
3.2 Traction forces impact on cell migration	29
3.3 Immunofluorescence (IF) staining	30

4 Discussion	31
4.1 <i>Behavior of urinary bladder cancer cell lines</i>	32
4.2 <i>Measured traction forces</i>	33
4.3 <i>Comparison of physical forces in cell sheets of urinary bladder cancer cells and keratinocytes</i>	33
4.4 <i>Using immunofluorescence to investigate possible stem cell markers</i>	34
5 Conclusion	34
6 Future perspectives	35
References	36
Appendix A: Recipe for PBS buffer	39
Appendix B: Python-based scripts.....	40
Appendix C: Complementary result of cell migration pattern of asynchronously growing cancer cells.....	52
Appendix D: Complementary result of cell migration pattern of quiescent and re-stimulated cancer cells.....	53
Appendix E: Information about the cell lines used in this project	55

Abstract

A broader knowledge on how cancer cells behave physically is important for understanding how they spread throughout the body. In order to understand how metastasis of cancer cells really works, it is necessary to know what happens with physical forces when cancer cells are awakened from quiescence. The project involved mapping of physical forces and dynamics in cancer cell lines, isolated from three patients with urinary bladder cancer (TCC).

Cell migration patterns and intercellular physical forces (traction forces) of re-stimulated cancer cells, after serum deprivation, was monitored by live cell imaging. The cell lines SW780, 5637, and T24 were starved to establish a quiescent cell state, and then re-stimulated with FBS before image acquisition. The magnitude and directionality of cell migration were slightly different between the cell lines. It was observed that cells of the T24 cell line migrated as single cells. The SW780 showed a pattern of collective migration, and the 5637 cell line had a partial collective migration. The results further showed an increase in traction forces directly after serum-stimulation of quiescent cancer cells. This is similar to a previous study of keratinocytes. A flower-like structure in SW780 cell sheets appeared after serum re-stimulation, which were investigated for the presence of stem cell markers.

The cancer cell lines showed common features when it comes to traction forces arising after exit from quiescence and activation of cell migration. However, different migration patterns, in terms of single-cell and collective migration, as well as different migration velocities were observed.

Abbreviations

AJCC	American Joint Committee	TCC	Transitional cell carcinoma
BSA	Bovine Serum Albumin	TEMED	Tetramethylenediamine
DAPI	4',6- diamidino-2-phenylindole	TFM	Traction force microscopy
DMEM	Dulbecco's Modified Eagle Medium	UV	Ultraviolet
DNA	Deoxyribonucleic acid	WLL	White light continuous laser
EDTA	Ethylenediamine-tetraacetic acid	2D	Two-dimensional
EMT	Epithelial-mesenchymal transition	3D	Three-dimensional
FBS	Fetal bovine serum		
G phase	Gap phase		
hrs	Hours		
IF	Immunofluorescence		
LED	Light-emitting diodes		
nm	Nanometers		
min	Minute		
MIP	Maximal intensity projection		
M phase	Mitotic phase		
PAA	Polyacrylamide		
PBS	Phosphate-buffered Saline		
PFA	Paraformaldehyde		
PIV	Particle image velocimetry		
RPMI	Roswell Park Memorial Institute		
Sulfo-SANPAH	Sulfosuccinimidyl 6-(4'-azido-2'-nitrophenylamino)		
S phase	Synthesis phase		

1 Introduction

1.1 Cell cycle

There has been estimated that the human body consists of 30 trillion cells with different structures and functions. Many of these cells are continuously renewed as a consequence of the cell cycle and cell death (Gregers, 2020). Only a few cells in the body do not divide at all like neurons, gametes and fully developed heart cells (Frade & Ovejero-Benito, 2015).

The cell cycle is divided into two phases, the interphase and the mitotic phase (M phase). The interphase is again divided into three phases (see figure 1). The first phase is called G_1 , and this is when the cells grow, the organelles are copied, and other molecular building blocks are made. Subsequently, cells enter the S phase, which is the phase of DNA synthesis. A complete copy of the DNA is built and centrosomes that will be used in the M phase are made. The third phase is called the G_2 phase. At this point, the cell growth continues, and proteins are synthesized in preparation for mitosis. The end of the G_2 phase is where the mitosis, and M phase starts, resulting in two daughter cells (Cooper, 2000).

In mitosis, the cells go through five different phases. In prophase, the chromosomes are being condensed, the mitotic spindle is formed, and the centrosomes move away from each other. In prometaphase, the nuclear membrane breaks down, and the chromosomes attach to the mitotic spindle. In metaphase, the chromosomes are lined up in the middle of the mitotic spindle, called the metaphase plate. In anaphase, the sister chromatids are separated and pulled towards opposite ends of the cell. And finally, in telophase, the nuclear membrane is formed again, and the division of the cytoplasm starts. In cytokinesis, the cytoplasm splits into two new cells. The cytoplasm is divided by a contractile ring made of actin and myosin filaments. The ring pinches the cell into two identical daughter cells (McIntosh, 2016). The cell cycle usually takes around 24 hours, but this can vary between cell lines. The time used for completion of one cell cycle is 21, 23, and 38 hours (hrs) respectively for the T24, 5637, and SW780 cell lines used in this research project.

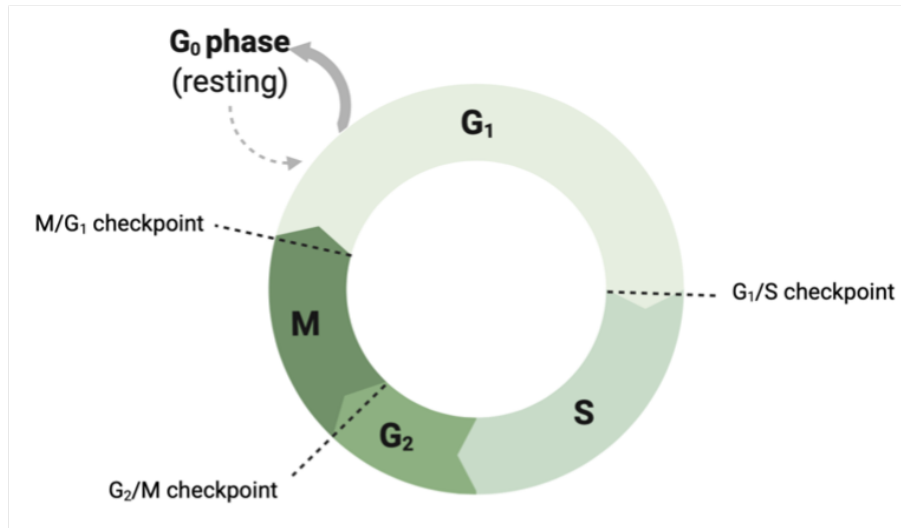


Figure 1: The cell cycle. Illustration of the cell cycle. The interphase includes the phases G_1 , S and G_2 while the M phase includes mitosis and cytokinesis. Cells can exit the cell cycle and enter the G_0 /resting phase (Lillebø, made in Biorender).

1.1.1 Quiescence

Quiescence is a state where cells are not dividing and is therefore not a part of the cell cycle. This happens due to changes in the microenvironment of the cell. When a cell exit the cell cycle in G_1 phase it enters a resting state called G_0 or quiescence. However, the cell has the capacity to re-enter the cell cycle, when exposed to different compounds that stimulate mitosis (mitogens) (see Figure 2) (Marescal & Cheeseman, 2020).

Many different cell types in our body are able to exit the cell cycle and enter quiescence, such as skin cells (keratinocytes), stem cells (blood, intestine), immune cells, and fibroblasts (connective tissue). Fibroblasts are for example activated during wound repair, resulting in cell migration and cell division at the wounded area (Grendler et al., 2019). Furthermore, quiescent lymphocytes are activated as part of the acute adaptive immune response (Kan & Hodgkin, 2014). In addition, quiescence is vital for cancer cells to gain further mutations that will help them survive in new surroundings and initiate metastasis. Further, cancer cells (cancer stem cells) do this to evade the effect of cancer therapy, which in general targets all dividing cells (Recasens & Munoz, 2019, Fiore et al., 2018).

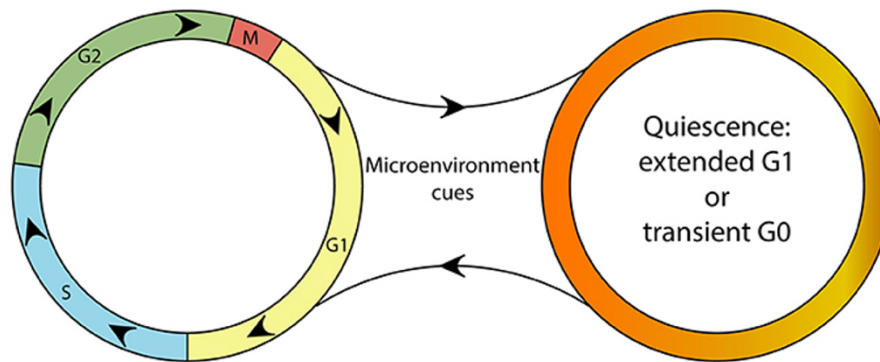


Figure 2: Schematic representation of the cell cycle as a continuous process, and the quiescence compartment as a separate state. The circle to the left illustrates a cell cycle including the phases M, G₁, S and G₂. The circle to the right shows the cells that have exited the cell cycle and entered the quiescent state (Fiore et al., 2018).

1.2 Cell migration

Cell migration plays an essential role in numerous physiological and pathological processes, such as during development, tissue remodeling, immune response, wound healing, and cancer spreading (Scarpa & Mayor, 2016). The cells either move as an individual single cell or as a unit of collective cells. Single cells migrate without cell-to-cell interaction (Ridley et al., 2003), while cells moving in groups maintain their cell-to-cell interactions and migrate coordinately within the group (Friedl & Gilmour, 2009).

The cytoskeleton is fundamental for cell movement. The cytoskeleton is built up of three basic filament structures; actin filaments, microtubules, and intermediate filaments. In addition, a variety of cytoskeletal accessory proteins, like motor proteins, are also required for proper cell migration (Alberts, et al., 2019). Cell polarization is essential for cell migration, since it helps the cell to determine the direction of its movements (Pandya et al., 2017). Cell migrations often occur in response to specific external stimuli, including chemical (Mak et al., 2016) and mechanical signals (Te Boekhorst et al., 2016).

1.2.1 Collective migration (of keratinocytes)

Collective cell migration is the process where a group of cells move together with the same speed and direction as a coordinated multicellular unit, over a period of time (Desai et al., 2013). Exit from quiescence is often associated with cells starting to migrate and later on divide. Keratinocytes and fibroblasts are for example cells that start to migrate and divide in conjunction to wound healing (Pastar et al., 2014). Stig Ove Bøe's research group has recently

shown that quiescent human keratinocyte monolayers show collective migration on a large scale after being activated by serum. This migration pattern appears to be linked to an increase in intercellular tension (stress in the cell sheet) directly after stimulation of cells with serum. The observed tension (forces) decreases at the same time as the start of cell migration (as shown in figure 3) (Lång, et al., 2021). The purpose of this project was to determine whether a similar mechanism can be found in other cell types.

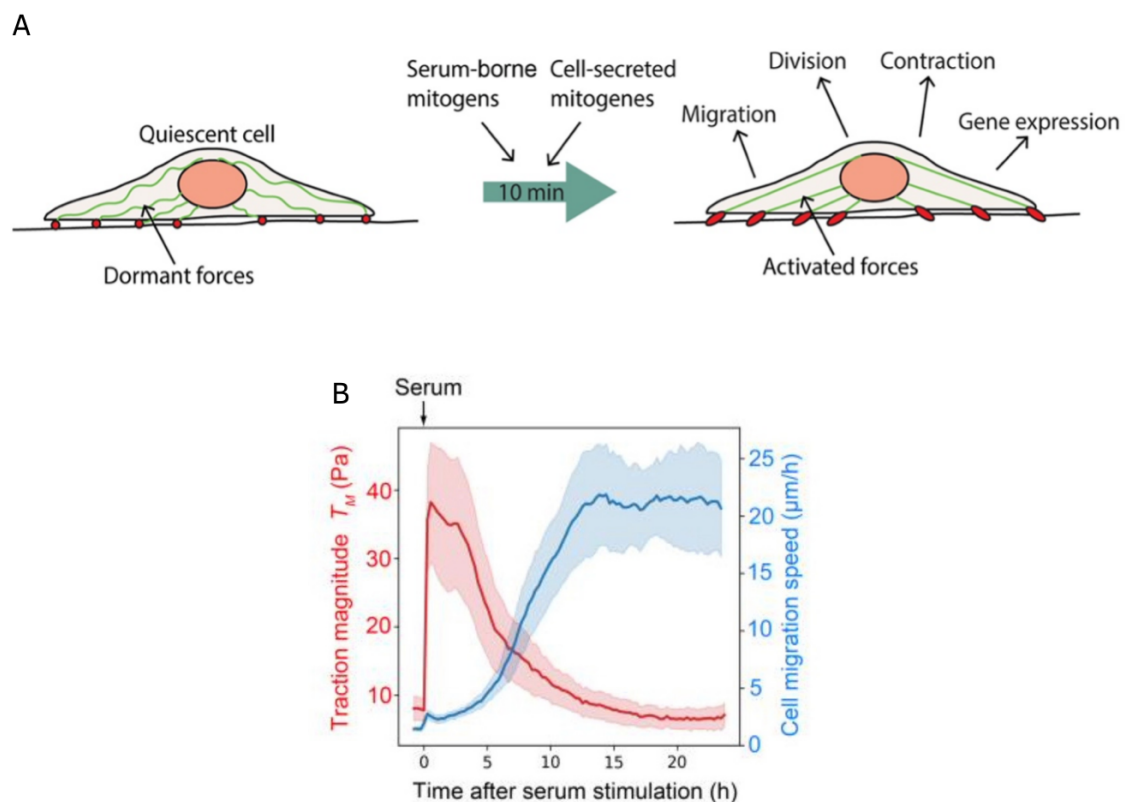


Figure 3: (A) The difference in forces between a quiescent cell and a cell that exits quiescence due to stimuli (FBS). (B) Results from migration and traction force microscopy experiment performed in a previous study (Lång, et al., 2021). The dark lines show the mean values, and the lighter areas around shows the standard deviation. The black arrow indicates the time of stimulation with FBS.

1.3 Cancer

There are several differences between normal cells and cancer cells. One important difference is cell signaling. While normal cells only grow after receiving signals telling them to grow, cancer cells might grow and divide in the absence of such signals. The cancer cells can also ignore signals telling them to stop growing or die (apoptosis) (Mohammad et al., 2015). Further, cancer cells have the ability to survive in blood vessels and spread to other tissues where the

cells normally do not grow (metastasis). All these features are a consequence of changes in genes that control how the cells function including growth, division, death, and cell signaling (Alberts, et al., 2019). Thus, anti-cancer therapy usually focuses on stopping cell division and/or cell migration.

1.4 Urinary bladder anatomy

Since the focus of this research project is on cancer cells originating from the urinary bladder, we will now briefly discuss this organ. The urinary bladder (figure 4) is a muscular pouch in the pelvis. The shape and size of the urinary bladder varies, depending on how full it is and pressure from the surroundings. When empty, the urinary bladder is roughly the size and shape of a pear. A normal bladder of an adult can store up to 400-600 mL of urine and makes it possible for urination to be infrequent and controlled (Holck, 2021).

The urine enters the bladder through the ureters and exits through the urethra. The musculature of the bladder is essential when it comes to the storage and excretion of urine. The bladder wall contains a specialized smooth muscle to make it capable of contracting during urination. The muscle fibers are directed in different ways to maintain structural integrity when the bladder is being stretched (Shermadou et al., 2022).

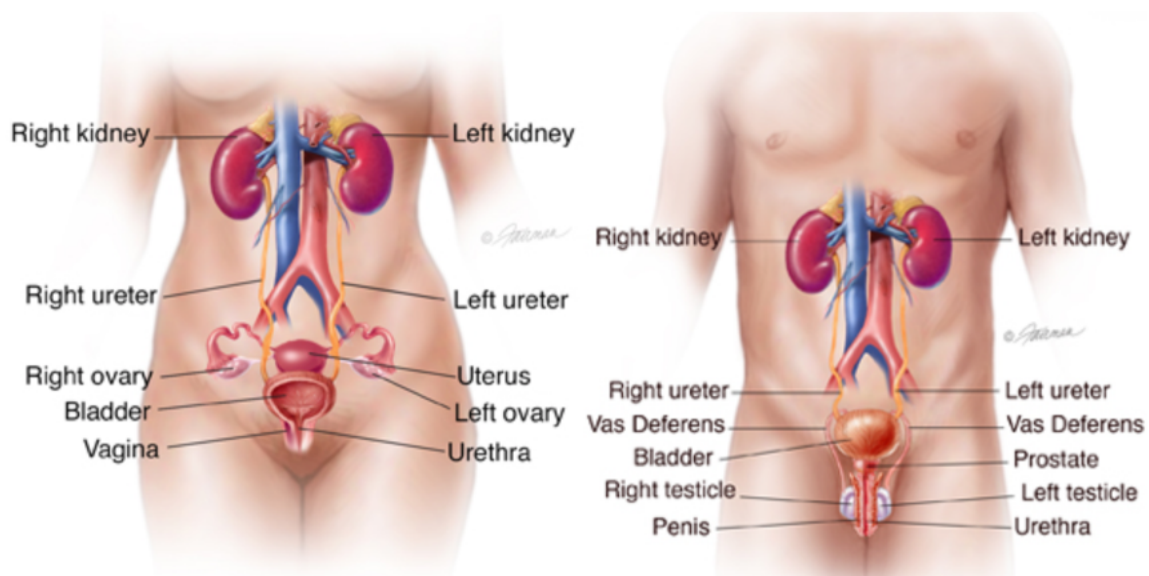


Figure 4: An overview of the female and male urinary tracts (Urology Care Foundation, n.d.).

1.5 Urinary bladder cancer

There are different types of bladder cancers. However, the most common type of bladder cancer is urothelial carcinomas, also called transitional cell carcinomas (TCC). This type of cancer starts in the urothelium which is an epithelial tissue consisting of many layers of epithelial cells that line the inside of the bladder (Kang, 2018). Urinary bladder accounts for about 3% of the cancer diagnoses in the world. Around 90% of urinary bladder cancer diagnoses occur in patients that are 55 years or older. The disease is also four times more common in men than women (Saginala et al., 2020).

Urinary bladder cancer is the unregulated growth of cancerous cells on the bladder wall's inner lining, which may cause different symptoms (Michaud et al., 1999). The most important sign of bladder cancer is hematuria, the presence of blood in the urine. This may also be caused by other diseases or health problems and should not be ignored. Other signs that might be caused by bladder cancer are having trouble urinating, pain during urination, or frequent, uncontrolled urination (Zhou et al., 2015).

The main procedure for identifying bladder cancer is cystoscopy. A hollow tube equipped with a lens, a cystoscope, is used to inspect the inside of the bladder. If the process is done under anesthesia, a biopsy will be taken. Later, the tissue sample will be carefully examined under a microscope for eventual signs of cancer. If signs of cancer are detected, the tumor will be removed and analyzed to determine a diagnosis, and the stage of cancer will be determined (Sanli et al., 2017).

1.5.1 Stages of urinary bladder cancer

The American Joint Committee on Cancer (AJCC) created the TNM system to stage cancer (shown in table 1). The T explains how far the cancer has spread throughout the bladder and if it has spread to any adjacent tissue. The N describes if cancer has spread to lymph nodes nearby the bladder. Lastly, the M describes if the cancer has spread to organs or lymph nodes far away from the bladder (metastasized). For staging cancer, the determined letter will be followed by a number between a and IV (zero and four) that will describe how far cancer has spread. Figure 5 shows the staging of cancer in the urinary bladder (DeGeorge et al., 2017).

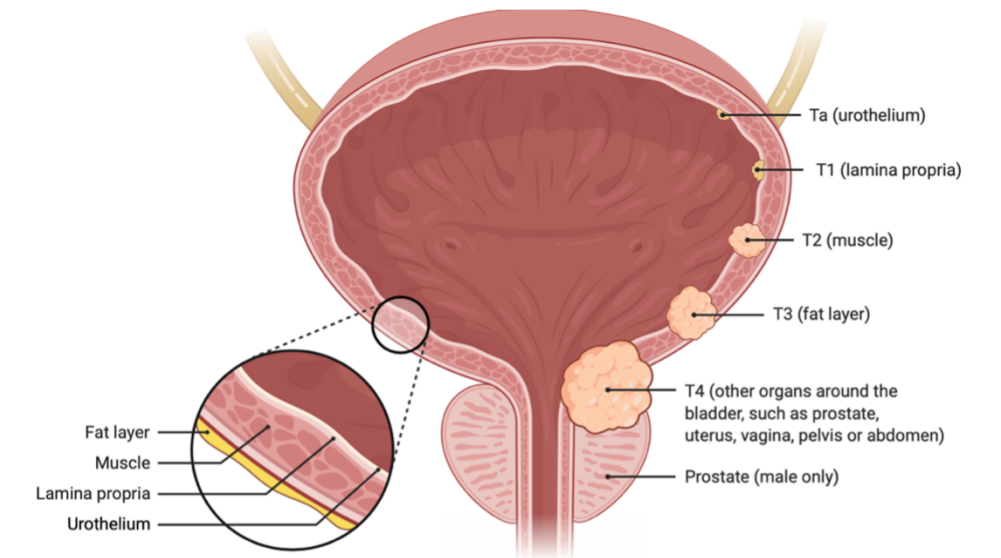


Figure 5: Bladder cancer staging. Cancer has different stages, from Ta to T4, as illustrated. The T explains that the cancer is spread in the bladder, but not into the lymph nodes or other areas of the body, while the numbers describe how far the cancer has spread throughout the bladder. Created with BioRender.com

Table 1: TNM, the American Joint Committee staging system of cancer. Table inspired by DeGeorge et al. (2017).

	<i>T (primary tumor)</i>	<i>N (regional lymph nodes)</i>	<i>M (distant metastasis)</i>
<i>0</i>	No evidence of primary tumor	No lymph node metastasis	No distant metastasis
<i>I</i>	Tumor invades subepithelial connective tissue	Single regional lymph node metastasis in true pelvis	Distant metastasis
<i>II</i>	Tumor invades muscularis propria	Multiple regional lymph node metastasis in true pelvis	
<i>III</i>	Tumor invades perivesical tissue	Metastasis to common iliac lymph nodes	
<i>IV</i>	Tumor invades any of the following: prostate, uterus, vagina, pelvic wall, abdominal wall		

1.6 Fluorescence in Biological Research

Fluorescence labeling of cells is used to visualize structures of interest using different types of microscopes (fluorescence microscopy). When exposed to light fluorescent probes or fluorophores absorb photons, resulting in electrons entering an excited state. As the fluorophores lose energy during vibrational relaxation, their electrons return to their ground state and a less energetic photon is emitted (fluorescence) (figure 6). Depending on the wavelength of the emitted light, it is either visible to the human eye, with a wavelength between 380 and 700 nanometers (nm), or detectable only by infrared cameras with

wavelengths above 700 nm (Schouw et al., 2021). Fluorescence is used to study molecular processes and is involved in nearly all forms of microscopy.

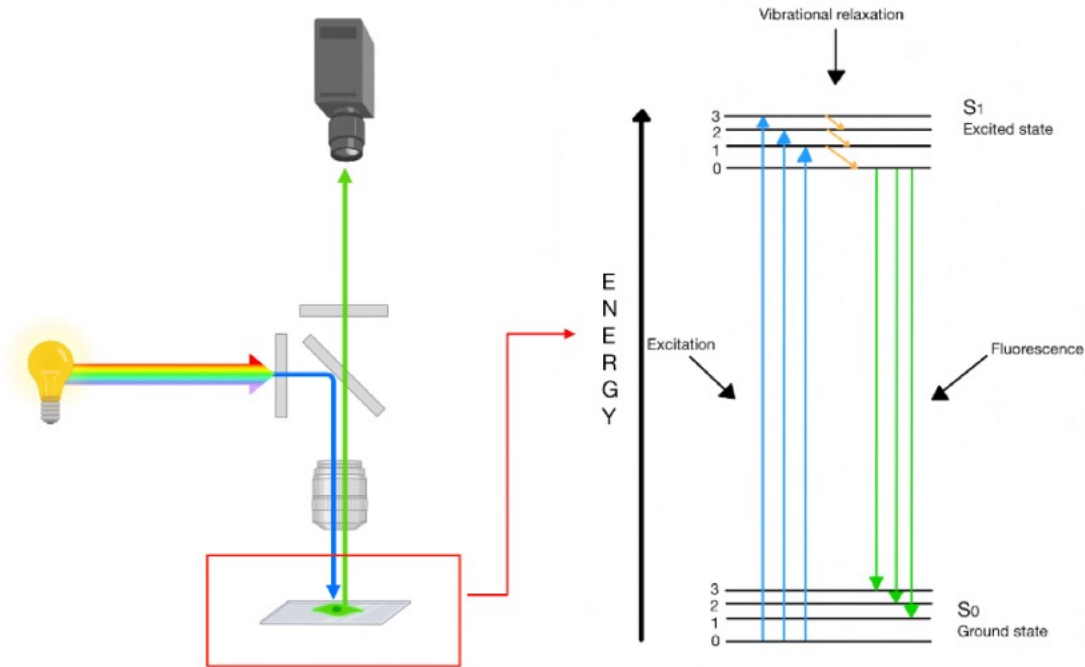


Figure 6: Fluorescent imaging and the concept of fluorescence. On the left is the light source of a microscope and the illustration shows how the direction of the light changes before it reaches the sample (blue line) and then is directed towards the detector/camera (green light). The right part of the image illustrates the different energy states the molecule (fluorophore) goes through. The blue arrows show the excitation, whereas the green lines show the emission. Created with BioRender.com, inspired by Schouw et al. (2021).

1.7 Microscopy and cell imaging

Microscopy refers to the methods used to obtain images of objects so small that they are not visible to the human eye. Microscopes can use either light or electron beams to visualize objects (light and electron microscopy respectively) (Meisslitzer-Ruppitsch et al., 2009). Today, many light microscopes use light-emitting diodes (LED) as the light source. This is because of the high efficiency and brightness that LED has reached, and also the LEDs capability of operating at low temperatures. Another advantage of LED illumination in fluorescence microscopy is that all variations of the semiconductor-based devices have a similar energy conversion efficiency with emission limited to a narrow range of wavelengths (Wessels et al., 2012).

Different types of microscopy techniques can be used in order to detect a variety of characteristics in tissues and cells. Among these are widefield and confocal microscopy most

commonly used for producing 2D images (Sanderson et al., 2014). Furthermore, 3D views of a sample can be achieved by acquiring Z-stack images. A conventional light microscope (widefield) illuminates a small area of sample at a time, but the reflected, fluorescent light can lead to "noise," which may compromise the image quality. By adding a small pinhole in the light path, confocal microscopy is able to eliminate this problem by passing only the light that emits from the desired focus point through the pinhole and to the detector/camera. The pinhole blocks any light outside the focus of attention. During confocal microscopy, light is focused onto a tissue sample, producing a virtual slice or plane that makes it possible to get images from a plane some micrometers into the sample. (Molecular Devices, n.d.). Images are of high-resolution quality with fine detail and more contrast than conventional widefield microscopy. When multiple sections are combined, the imaging technique allows the reconstruction of virtual three-dimensional images of the tissue (Nwaneshiudu et al., 2012).

The overview below shows a high-content imaging microscope. High-content imaging means that a large amount of data can be collected over time (Joshi & Lee, 2015). The ImageXpress Micro Confocal High-Content Imaging System (shown in figure 7) is an example of this kind of imaging. It is an automated microscope that can shift between confocal and widefield imaging of both fixed and live cells. This microscope can be used for tracking cell migration since it can acquire images of many samples (relatively fast) over time and collect a large amount of data (Molecular Devices, n.d.).

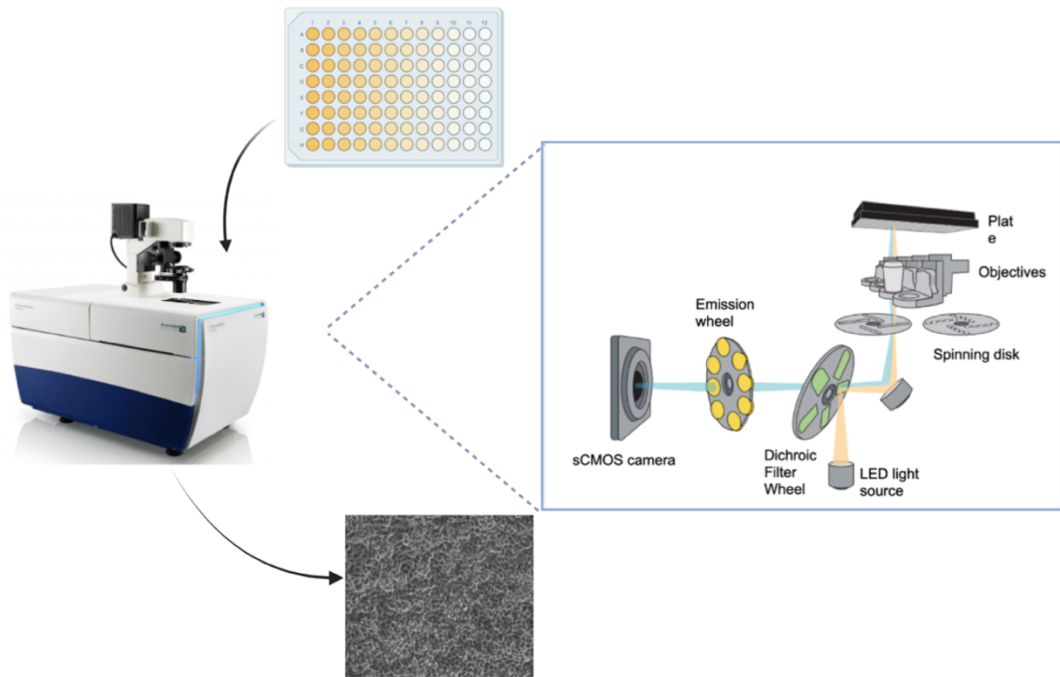


Figure 7: High-Content imaging microscopy. Illustration showing where the 96-well plate goes into the microscope, what happens inside of the microscope and what an acquired phase contrast image (transmitted light) can look like (Lillebø, made in Biorender).

1.7.1 Traction force microscopy

Traction force microscopy (TFM) is a method used to study mechanical forces in different experimental systems. For example, measure the forces a migrating cell exerts on its substrate (Lekka et al., 2021). The principle of TFM (shown in figure 8) is that cells are seeded on an elastic substrate, like a polyacrylamide gel, with fluorescent beads embedded in it. Forces on the substrate, caused by the migrating cells, result in deformation of the gel and displacement of the beads. The bead displacements can be recorded in a microscope, followed by calculation of traction forces using extensive computer algorithms (Bauer et al., 2021).

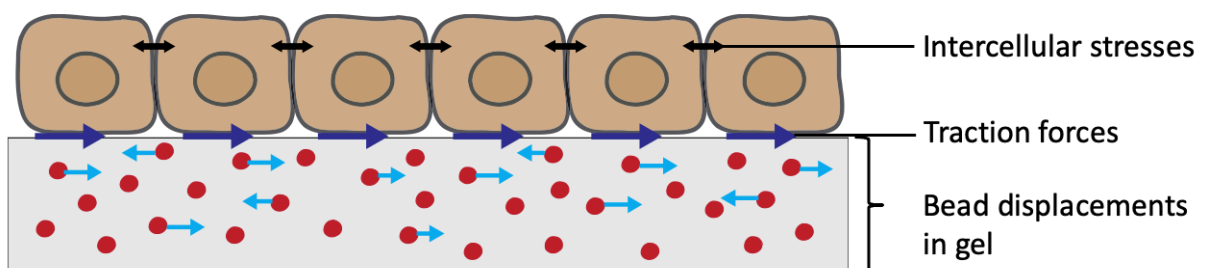


Figure 8: Overview of Traction Force Microscopy (TFM). This method is for example used to measure the forces a migrating cell exerts on its substrate. Cell migration creates bead displacements in polyacrylamide gel, allowing calculations of traction forces in substrate. Illustration with the courtesy of Anna Lång, inspired by Ulrich S. Schwarz (2015).

1.8 Aims of the thesis

The aim of this research project was to understand how changes in physical forces are coupled to molecular mechanisms that drive mechanical processes like cell migration and tissue remodeling. It has been shown that monolayers of quiescent human keratinocytes show collective migration after stimulation with serum. Prior to cell migration, an amplification of traction forces appears in the cell sheet (Lång et al., 2018). Our aim was to discover if the same pattern could be found in other cell types, and if this is a general mechanism of cells that exit quiescence. To do so, we performed microscopy-based methodologies for mapping physiological forces and dynamics in living cells originating from urinary bladder cancer patients.

2 Materials and methods

2.1 Cell culture

2.1.1 Cell lines and culture conditions

Three different urinary bladder cancer cell lines were used in this project. The cell lines are SW780 (CRL-2169™; ATCC), 5637 (HBT-9™; ATCC), and T24 (HBT-4™; ATCC), and they all originate from human urothelial carcinomas.

The optimal incubation growth conditions for these cell lines are 37 °C and 5% CO₂. The SW780 cell line was cultured in Dulbecco's Modified Eagle Medium (DMEM; Gibco™), 5637 in RPMI 1640 with L-glutamine (L0500-500; Biowest), and T24 in McCoy's 5A (modified) medium (12330031; Gibco™). Each medium was supplemented with 10% fetal bovine serum (FBS; Sigma-Aldrich) as nutrition, and 1% penicillin/streptomycin (PenStrep; Gibco™) to prevent bacterial growth.

2.1.2 Cell cultivation and passaging

The cultivation of the cancer cells was done in T75 cell culture flasks (156499; Thermo Fisher Scientific) with the preferred growth medium (see section 2.1.1). Cell cultivation was done by regularly passaging of cells and daily monitoring them to ensure an optimal growth rate and high cell viability. The cells were monitored daily by observing the color and the clearness of

the growth medium to ensure that the culture was not contaminated. As well as ensure that there were mitotic cells and few dead cells in the culture flasks.

The cancer cell lines were passaged when the culture reached 70 – 90% confluence. Firstly, the growth medium in the T75 flasks was removed and cells washed twice with 6 mL of pre-warmed PBS (PBS, Appendix A). Washing with PBS contributed to the removal of dead cells and FBS (which would otherwise inhibit the effect of trypsin on the cells). Secondly, the cells were trypsinized using 2 mL of trypsin (0,05% Trypsin-EDTA (1X); Gibco™) in order to detach the cells from the plastic surface. The cells were then placed in the incubator until detached from the surface. This process was monitored under the microscope, and when the cells were rounded up and floating around by tapping or tilting on the flask, 8 mL of pre-warmed growth medium with 10% FBS was added to neutralize the trypsin. Medium and trypsin were resuspended with a pipette to separate the cell clumps into single cells. Finally, the cells were splitted in a ratio of 1:5 in a total volume of 15 mL. However, when the culture does not reach the desired confluence, the range for splitting cells was 1:2 and to 1:5.

2.2 Live cell imaging of migration pattern

Several migration assays were performed. These experiments aimed to inspect the migration pattern of the cell lines before and after starvation, and re-stimulation. The cell lines were either exposed to serum deprivation and then re-stimulated with growth mediums containing 15% FBS, or seeded in 96 well plate with normal growth medium (no starvation). These live cell migration experiments were performed in the following steps (see figure 9); collagen IV coating of multiwell plates, cell counting, diluting cell solutions, cell seeding in plates, cell starvation, re-stimulation with serum, and finally live cell microscopy. Live cell imaging was performed using the ImageXpress® Micro Confocal high-content Imaging System (Molecular Devices).

2.2.1 Collagen IV coating

Prior to live cell imaging experiments, the 96-well Greiner Sensoplates with glass bottom (M4187-16EA, Merck Life Science (#655892, Greiner Bio-One)) were coated with collagen IV to ensure attachment of the cells to the glass surface. A solution of collagen IV was prepared by diluting the stock (1 mg/mL collagen IV, C7521, Merck) 1:50 in sterile PBS. The final concentration of collagen in each well was 20 µg/mL. 100 µL of the collagen IV solution was

transferred into each well and the plate sealed with parafilm to prevent evaporation of the solution. The plate was stored in the fridge overnight at 4°C, to ensure the collagen attach to the surface, and later cells have a layer of collagen to attach to. Before seeding of cells in the 96-well plates, described in section 2.2.3, each well was washed twice with 100 µL pre-warmed PBS to remove excess collagen IV.

2.2.2 Cell count estimation

Before seeding cells in the wells of a multiwell plate, or 6 cm dish, the number of cells had to be counted. The counting was done by the use of a Countess 3 Automated Cell Counter (AMQAX2000; Invitrogen, Thermo Fisher Scientific) and Trypan Blue Stain (0.4%, Invitrogen™). The primary purpose of the staining dye was to color dead cells, which provides accurate cell count and cell viability.

Prior to cell counting, the cells were treated with trypsin and resuspended in the respective growth medium as described in section 2.1.2. The cell suspension was resuspended to ensure a suspension of single cells before preparing the stained cell suspension mix. 20 µL of the cell suspension and 20 µL of Trypan Blue Stain were added into an Eppendorf tube, and the mixture was homogenized. 10 µL of the mix was transferred to each of the chambers of a disposable slide (Countess Cell Counting Chamber Slides, Invitrogen, Thermo Fisher Scientific). The disposable slide was placed in the cell counter, and the number of cells per mL was automatically estimated.

2.2.3 Cell seeding in 96-well plate

To execute seeding into a 96-well plate, the cells were washed and treated with trypsin, as described in section 2.1.2. Subsequently, the cells were counted to calculate the cell suspension and growth medium needed to have the desired number of cells in suspension. The intention was for the suspension to contain 600.000 cells in a volume of 900 µL, as shown in figure 9. To calculate the amount of cell suspension needed in the solution used for seeding, equation 1 was used.

$$\text{Volume of cell suspension} = \frac{\text{Number of desired cells}}{\text{Total cell count}} \quad (1)$$

By subtracting the volume of cell suspension from the total desired volume, 900 μL , the amount of growth medium needed is also revealed. The determined volume of cell suspension and growth medium was added to an Eppendorf tube to make the dilution series. The dilution series was created by adding 450 μL of growth medium to another eleven Eppendorf tubes and then transferring 450 μL of cell suspension from the first tube to the second, then mixing the cell suspension and growth medium by pipetting the solution repeatedly up and down. Subsequently, 450 μL of cell suspension in the second tube was transferred into the third tube and so on. When the dilution series was prepared, the PBS was removed from the wells, and 150 μL of each dilution series added to the respective wells, see figure 9.

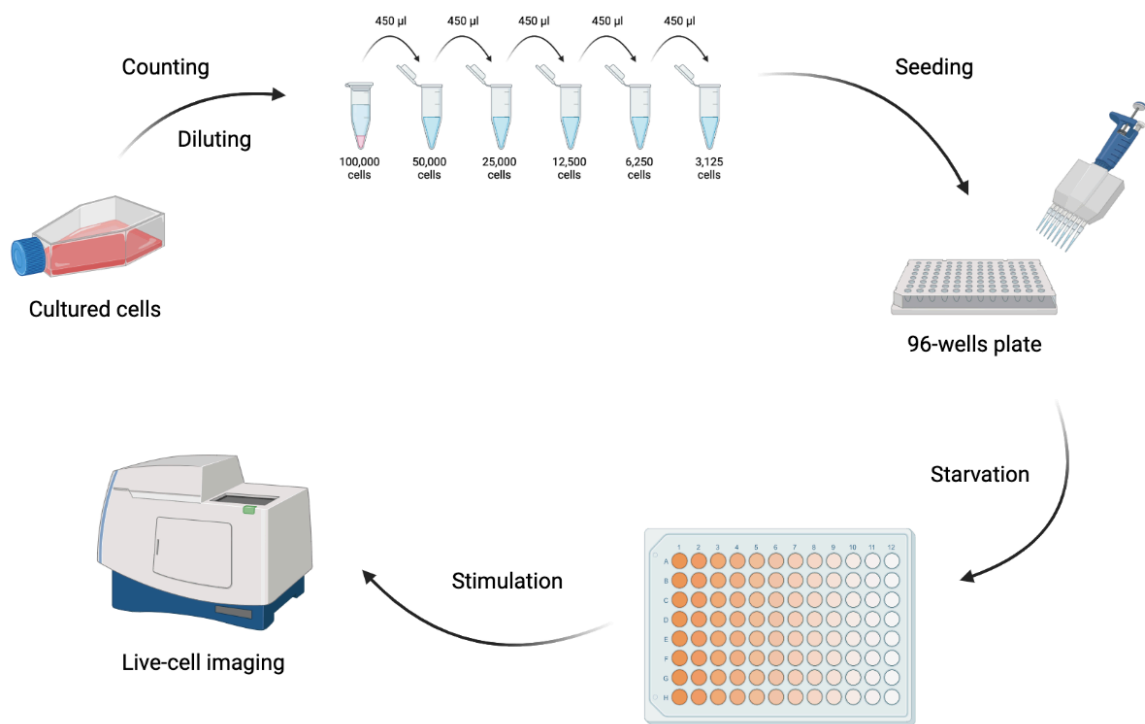


Figure 9: Illustration of the experimental setup of live cell migration experiments. The cultured cells were counted, then diluted to a desired number of cells. Cells were then seeded into a 96-well plate and incubated overnight to produce a confluent cell sheet. Moreover, the cells were starved to replicate quiescent cells before stimulation. The different shades of red in the figure demonstrate the dilution of cell numbers in each well. After stimulation, live cell imaging was performed to monitor cell movement. Created with BioRender.com

2.2.4 Cell starvation and re-stimulation of cells

Cell starvation by serum deprivation induces a cell state called quiescence, where the cells are non-dividing. Firstly, the cells were washed twice with pre-warmed serum-free medium, and then serum-free medium was added to each well. After changing to serum-free medium, the

starved cells in wells were placed in the incubator and cultured at 37 °C and 5% CO₂ for one week. Changing the growth medium was performed by using a multichannel pipette. This was done carefully, especially to avoid touching the bottom of the wells, because it could cause scratches in the cell sheet and affect the migration during live cell imaging.

Before performing live cell imaging, the starved cells in the 96-well plate were re-stimulated with serum-containing medium. The cells were washed with serum-containing medium using a multichannel pipette.

2.2.5 Live cell imaging microscopy

Live cell imaging was performed using the ImageXpress Micro Confocal high-content imaging microscope, controlled by the MetaXpress software (Molecular Devices). The system was equipped with a 20x Ph1 S Plan Fluor ELWD ADM 0.45 NA Nikon air objective with a phase contrast ring and transmitted light, and an environmental control gasket that maintains 37°C, proper humidity and 5% CO₂. Image acquisition was carried out in widefield mode, with a camera binning of 2 (pixel size of 3.367 μm x 3.367 μm). 4 sites per well were acquired during a period of 30 hrs and a time interval of 4 minutes was used. Acquired time lapse movies were analyzed using the TrackMate plugin in the Fiji Image J software (section 2.2.6).

The 96-well plate containing serum-stimulated cells was placed on the microscope stage and adopted to the microscope environment for 30 min prior to image acquisition. The plate must have the same temperature as the microscope to ensure optimized focusing during acquisition. Temperature changes in the plate and/or instrument will affect the focusing on the samples and the quality of the data and data analysis.

2.2.6 Image processing

The acquired images for each well, generated from the ImageXpress Micro Confocal Microscope, were organized in time points. Images were sorted by placing all time points from one well in the same folder by using the Python-based script, `file_sorting.py` (Appendix B.1). Moreover, the data could be transported to Fiji ImageJ software (Tinevez, 2017) for further analysis. Fiji ImageJ offers different features for image adjustment; performing manual tracking of cell movements, visualizing cell migration patterns, generating combined movie files, and

more. Cell migration patterns were further analyzed using manual tracking with the TrackMate plugin in Fiji ImageJ (Fazeli, 2020). Graphs showing average cell migration speed over time were generated using an in-house Python-based script (Appendix B.2).

2.2.7 PIV analysis

PIV (Particle image velocimetry) analysis was performed in order to describe the magnitude and directionality of cell migration. The cells were observed in ImageXpress Micro Confocal high-content imaging microscope (Molecular Devices) as mentioned in section 2.2.5. The data obtained were analyzed with in-house Python-based scripts using PyCharm. The scripts used for the analysis were `file_sorting.py` and `PIV_batch.py`, all of the scripts can be found in appendix B.

The single images acquired from MetaXpress software were sorted as mentioned in section 2.2.6 above. Analyses were performed within a selected rectangular area of each single image. Within this area, vectors were generated to visualize the velocity fields at a given time point after stimulation, as well as the migrating direction and speed of the cells in the cell sheet.

2.3 Traction forces in cell monolayers

The Traction force microscopy experiment was performed corresponding to the protocol modified by Lång, 2021.

2.3.1 Preparation of collagen IV-coated polyacrylamide gels

Collagen IV-coated polyacrylamide (PAA) gels were prepared in a 12-well glass bottom multiwell plate (P12G-1.5-14-F, MatTek Corporation). A mixture of Bind-Silane (GE17-1330-01, Merck) : ethanol : acetic acid at a 1:12:1 ratio was mixed and transferred to the 12-well MatTEK plate, and activated the glass bottom for 4 min, then washed twice with absolute ethanol. 4.069 kPa polyacrylamide gels were prepared by mixing 93.75 μ l 40% (7.5%) acrylamide solution (161-0140, BioRad), 37.5 μ l 2% (0.15%) Bis-solution (161-0142, BioRad), 2 μ l (0.4%) Carboxylate-modified fluorescent latex beads (FluoSpheresTM Carboxylate-Modified, 0.2 μ m, 580/605; F8810, Molecular Probes), 2.5 μ l 10% Ammonium Persulfate (APS, 0.05%, BioRad), 0.25 μ l 100% tetramethylenediamine (TEMED, 0.05%, T-9281, Sigma) and 364 μ l LMQ-H₂O. 15 μ l gel

solution was transferred to each well and then covered with a 12 mm in diameter, circled GelBond film (801129833, Cytiva), with the hydrophobic side facing down.

The gels in the 12-well MatTek plate were polymerized for 40 min upside down. 2 mL 10x PBS was added to each well, then rested for 40 min before removing the GelBond films. Gels were then washed twice with 1x PBS in 4 min each time, and then treated with 40 μ l 4% Sulfo-SANPAH ((sulfosuccinimidyl 6-(4'-azido-2'-nitrophenylamino) hexanoate (22589; Thermo Fisher Scientific™) for 4 min under UV light. The used Sulfo-SANPAH was replaced with fresh Sulfo-SANPAH, and again treated with UV-light for 6 min. Subsequently, the Sulfo-SANPAH was removed and the gels were washed twice with 1x PBS in 4 min each time, and then coated with 0.1 mg/mL collagen IV (C7521, Merck), and stored at 4 °C overnight. Prior to Traction force microscopy (TFM) experiment, the gels were washed twice in 1x PBS and then stored at 4 °C in 1x PBS.

2.3.2 Cell seeding on polyacrylamide gels

Cell seeding in 12-well MatTEK plate was performed as described in section 2.2.2. However, the desired number of cells in the first well was 400.000 cells in a volume of 2 mL, and the cell suspension was transferred directly into the well and filled with pre-warmed serum-containing medium. The number of cells was halved for each well it was transferred to. The number of cells in the respective wells were 200.000, 100.000 and 50.000. The day after seeding, cells were put on serum-free medium and kept in the incubator at 37 °C and 5% CO₂ for a week, prior to TFM.

2.3.3 Traction force microscopy (TFM)

The TFM experiment was performed using the Zeiss AxioObserver.Z1 microscope (Zeiss), controlled by the Zeiss Zen software. The microscope was equipped with a CO₂ incubation chamber, a Colibri 7 LED light source, and a 10x 0.5 NA FLUAR air objective. The 12-well MatTEK plate containing starved cells was placed on the microscope stage and adopted to the microscope environment for 1 h. We acquired z-stacks on the samples over time, using a fluorescence channel for detection of the beads (580/605 nm) and a phase contrast (transmitted light) channel for the cells. Moreover, to obtain a “before stimulation” reference,

3-4 consecutive frames, 16 min intervals between frames were captured. The imaging was then paused and 1 mL 30% FBS containing medium was added to each well in order to activate the cell sheets. After a 30h of imaging, we stopped the time lapse and trypsinized the cells to make them detach from the gel. We then acquire another round of z-stack images on the relaxed gel. These are then called reference images. For each time point, 4 sites per well were captured. The 10x objective generated a field of view of 1331×1331 μm and for each site a stack of 6 z-planes was collected with a z-step size of 2.2 μm . For each z-stack, the middle z-plane was focused at the center of the gel surface.

Calculation of traction forces for each site was done by a maximal intensity projection (MIP) algorithm. The bead displacement traction forces and tension maps were predicted using pyTFM (Bauer et al., 2021). Acquired time lapse images were subjected to image registration using the descriptor-based series registration plugin, macro_concatenate.ijm (Appendix B.3.1) and macro_TFM.ijm (Appendix B.3.2) in the Fiji Image J software. The registration plugin, macro_concatenate.ijm was used to combine “starved, activate 1, activate 2 and trypsin” files from respective sites into one time lapse per site. Additionally, macro_TMF.ijm removes the "trypsin" image from the rest of the respective time lapse. The bead displacement, traction forces and tension maps were predicted using open source codes from pyTFM (Appendix B.3.3).

2.4 Visualization of cancer cells by immunofluorescence (IF) staining

Visualization of actin networks, cell nucleus, and the detection of stem cell markers was done by immunofluorescence (IF) staining and confocal microscopy using the Leica TCS SP8 microscope (Leica Microsystems). The SW780 and T24 cell lines were fixed and then stained with different antibodies.

2.4.1 Preparation and fixation of cells for IF staining

Cells were grown, fixed, and stained with different antibodies on 12 mm round glass coverslips (VWR). Cell seeding and serum starvation in 6 cm Petri dishes (Falcon® Cell Culture Dish) were performed as described in section 2.2.3 and 2.2.4. However, cells were seeded in dishes with coverslips attached to the bottom of the dishes at 2.5 million cells in a total volume of 4 mL

medium per dish. Prior to the cell fixation, it was prepared starved cells and 24 h serum-stimulated cells of both cell lines.

The cell sheets on coverslips were fixed with 2 mL of 4% paraformaldehyde (PFA; 158127, Merck Life Science) for 10 min on ice. After fixation, cells were permeabilized in 2 mL of 0.25% Triton X-100 (T8787, Merck Life Science) for 4 min on ice, to open pores in the cell membrane. PBS (Appendix A) was the dilution medium for both reagents and was also used in the multiple washing steps required.

2.4.2 Protocol for IF staining

Before IF staining, fixed cells were treated with 0.5% Bovine serum albumin (BSA; Cohn fraction V, B2000, Saveen Werner AB) in PBS. BSA works as a guide, where it prevents antibodies from unspecific binding.

The primary antibodies used were Rabbit anti-Human SOX2 (ab97959; Abcam, 1:500) and Rat anti-Human Ki67 (14-5698-82; Thermo Fisher Scientific, 1:500). The secondary antibodies used were Goat anti-Rabbit Alexa Fluor 594 (A11037, Invitrogen, 1:200) and Goat anti-Rat Alexa Fluor 555 (A21434, Invitrogen, 1:200). All antibodies were diluted in 0.5% BSA. Initially, primary antibodies were added to the starved and re-stimulated cells. SOX2 was added to the first half of the samples, and Ki67 was added to the second half of the samples. Accordingly, the samples were placed in a refrigerator, at 4°C overnight. Subsequently, a repetitive process was done with the respective secondary antibodies and then incubated for 1 h at 37°C. The cells were then incubated with Phalloidin-iFluor 488 (ab176753, Abcam, 1:1000) at room temperature in the dark for 45 min. The fluorescent reagent contains Phalloidin conjugates that bind to actin filaments in the cells. Finally, the glass coverslips were attached to the microscope slide (Thermo Fisher Scientific) by using Vectashield® Antifade mounting medium with DAPI (4',6- diamidino-2-phenylindole; H-1200-10, Vector Laboratories). The medium sticks the cell sheets on the coverslips against the microscope slide. DAPI is a fluorescent DNA stain that colors the cell nuclei by binding to A-T regions of DNA. The coverslips were washed 2-4 times with PBS between each step from staining with antibodies and incubation with Phalloidin to assembling of coverslips to microscope slides.

2.4.3 Confocal microscopy

The Leica TCS SP8 microscope was equipped with a 40x 1.3 NA oil immersion objective, a white light continuous laser (WLL) and a 405 nm UV laser. The Phalloidin signal was detected with the 488 nm laser line using the WLL, and DAPI signal was detected with the 405 nm UV laser. The 594 and 555 nm WLL laser lines were used to detect SOX2 and Ki67 signals respectively. Image acquisition was performed sequentially for each channel using the 40x 1.3 NA oil immersion objective and hybrid detectors. Laser intensities were set for the FBS stimulated sample that showed the strongest fluorescence intensity in the 488 nm channel (Phalloidin). The instrument settings of Phalloidin and DAPI were kept constant throughout the experiment, while settings for the secondary antibody signals were switched, depending on the sample analyzed.

3 Results

To study if the mechanism seen in the monolayers of quiescent human keratinocytes is similar in other types of cells, urinary bladder cancer cell lines were starved for a week before they were re-stimulated. Experiments were performed with different concentrations of the cell lines 5637, T24, and SW780, seeded in collagen-coated wells and wells with polyacrylamide gels to examine cell migration and traction forces respectively.

3.1 Cell migration pattern

In order to observe the cell migration pattern, live cell imaging with widefield microscopy was used. The cells were stimulated after the quiescent cell state was established, and the cell movements were captured in the microscope for 24-30 hrs. The cell migration pattern was also visualized using PIV analysis of time lapse videos.

3.1.1 Cell migration patterns of asynchronously growing cancer cells

For the purpose of observing the difference between cell migration of cells growing in culture (asynchronous) and that of cells that had been starved and then re-stimulated, experiments were conducted in which cells were seeded in 96-well plates without starvation and then subjected to live cell imaging for 24 hrs. The graph in figure 10 shows the average speed of the cells over the course of 10 hrs. As can be seen in the graph, cell line 5637 migrates far more rapidly than the other cell lines in the experiment. The migration speed, however, was rather constant in cell cultures that have not been starved. This applies to all the three cell lines, which

is why they were analyzed for a shorter period of time compared to starved and re-stimulated cells.

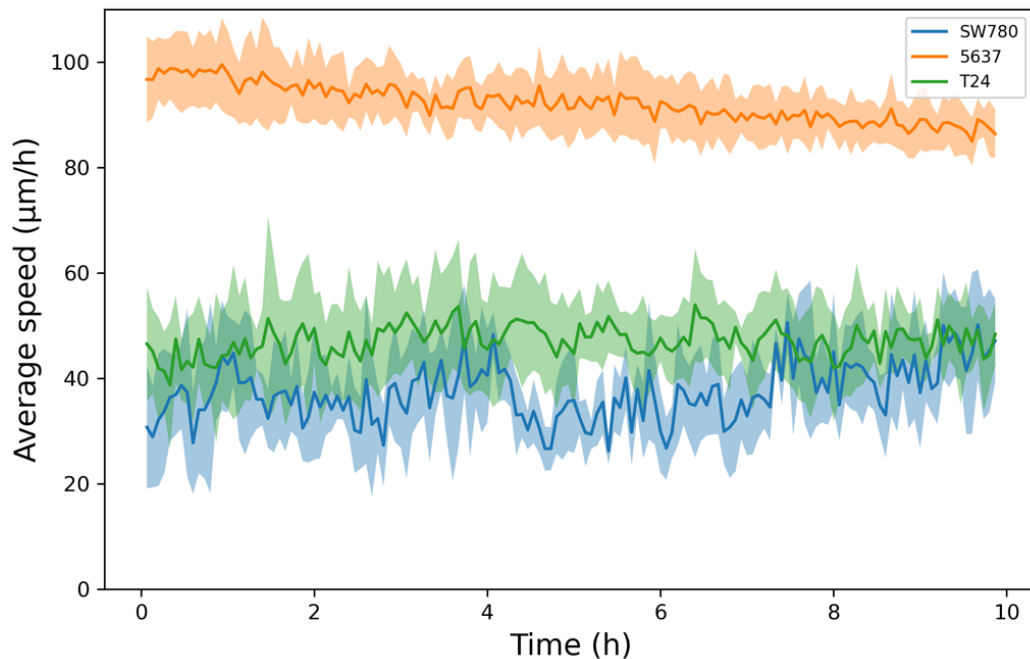


Figure 10: The average migration speed of the cell lines SW780 (blue), 5637 (orange), and T24 (green) over a ten-hour period. The mean values are shown as the dark lines, while the area of a lighter color is the standard deviation.

3.1.2 Cell migration patterns of quiescent and re-stimulated cancer cells

In order to observe the effect of quiescence on cell migration, experiments were conducted in which different concentrations of cells were starved for one week before being re-stimulated with FBS. This would induce quiescence in cells, that subsequently re-enter the cell cycle upon stimulation. To observe the migration of quiescent cells, images were acquired every fourth minute over a one-hour period. After that, the cells were stimulated with 15% FBS, and another round of time-lapse images was acquired for a period of 30 hrs so that the migration and initiation of cell division could be observed. Cell migration patterns were analyzed using manual tracking with the TrackMate plugin in Fiji ImageJ (Tinevez, 2017).

The results presented in figure 11, indicate that there is a velocity difference between quiescent cells and stimulated cells. The starved cells (figure 11A) have a relatively constant speed, similar to the cells that are growing asynchronously (figure 10). However, the migration speed was significantly lower and the difference between the cell lines is notably

smaller for the starved cells (compare figure 10 and 11A). The graph for the re-stimulated cells (figure 11B) shows a quick response in migration for the SW780 cell line. The response in the SW780 cell line was much faster than for the other two cell lines, however, both of the other cell lines show an increase in migration after stimulation. This response is similar to the one seen in keratinocytes, but not identical.

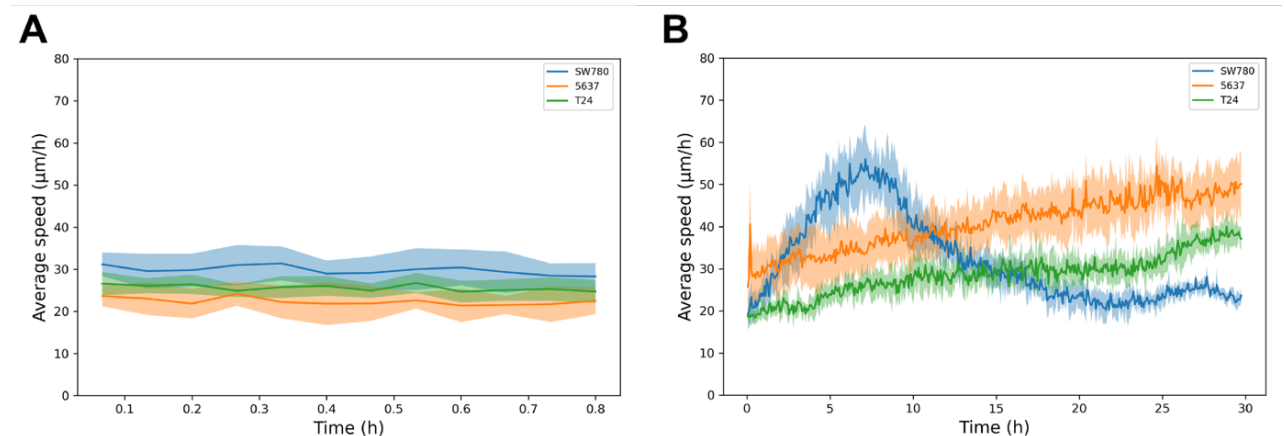


Figure 11: Starved and stimulated cell migration in quiescent cell sheets. The average speed (measured in $\mu\text{m}/\text{h}$) of the cell lines SW780 (blue), 5637 (orange), and T24 (green) over a 30 hrs period, in a density of 12.500 cells/well. The mean values are shown as the dark lines, while the area of a lighter color is the standard deviation.

After live cell imaging, the python-script in Appendix B.1 was used to sort the data. All the images from the same site of the same well were put together to make videos. The videos of the cells make it possible to see the migration pattern and direction. Representative time lapse videos were selected and PIV analysis performed using the in house python script Quiver.py (Appendix B.4). It was observed that cells of the T24 cell line migrated as single cells. The SW780 showed a pattern of collective migration, and lastly, the 5637 cell line had a partial collective migration, yet the cells did not move in a clear defined direction for longer periods of time. The movement of the cells is visualized in the graphs of figures 12, 13 and 14.

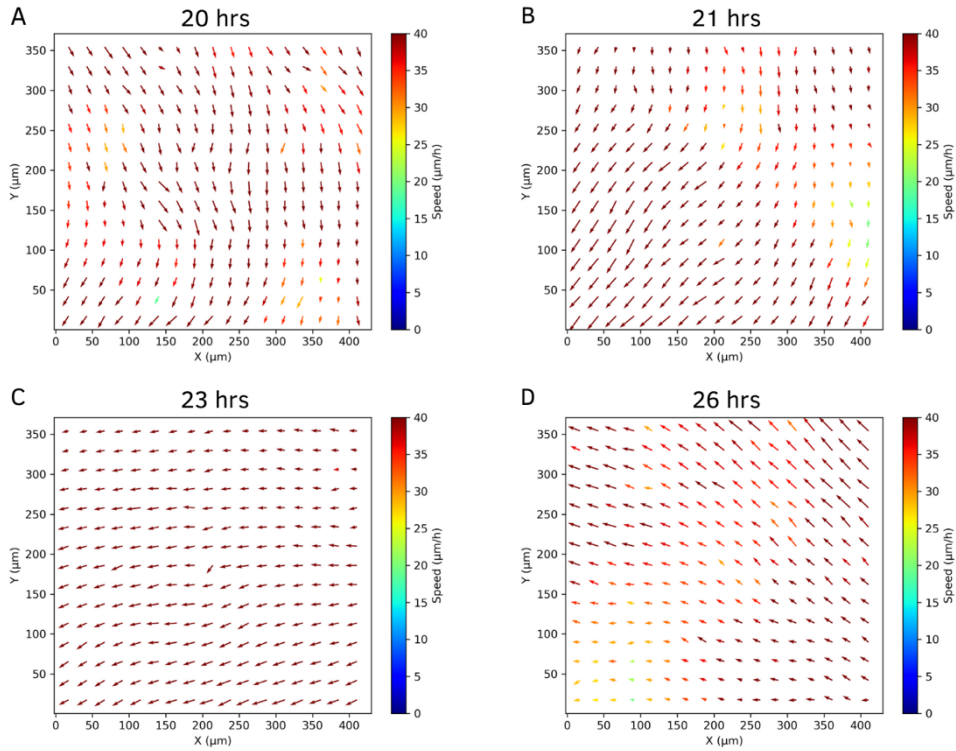


Figure 12: PIV graph showing cell migration of SW780. The migration pattern of the cells is illustrated as arrows, to show the direction and speed of cell movement at a given time point after stimulation. This plot is based on PIV analysis, where the vector components in the vector field are interpreted as cells in the cell sheet. The order of the graphs A to D is the order the images were taken in. The SW780 cells are clearly moving with collective migration throughout the hours of analysis.

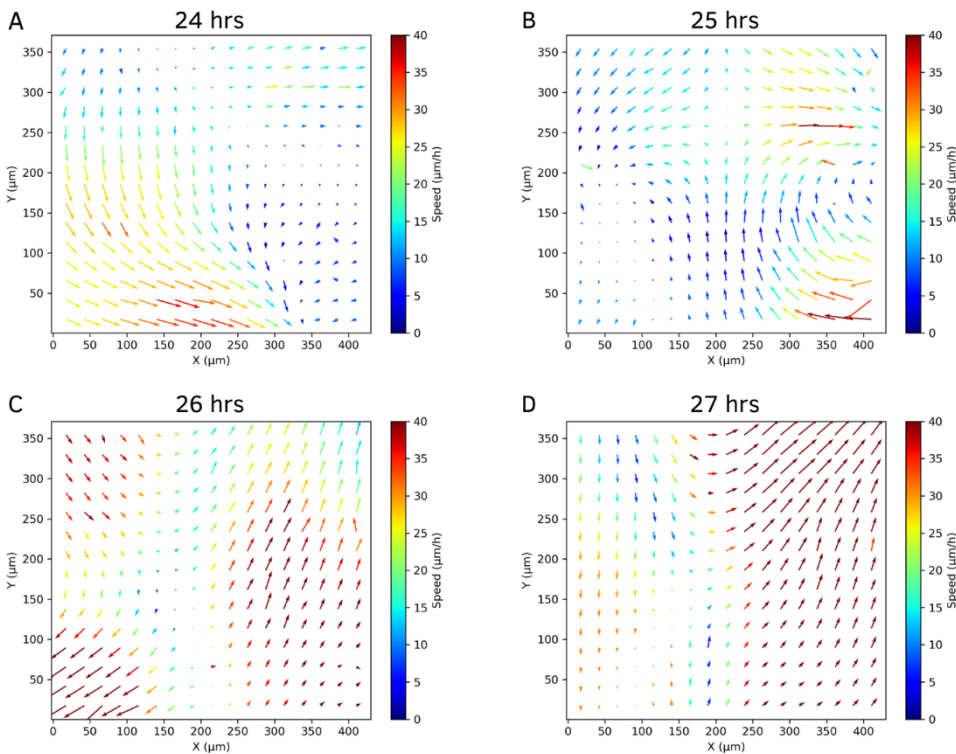


Figure 13: PIV graph showing cell migration of 5637. The migration pattern of the cells is illustrated as arrows, to show the direction and speed of cell movement at a given time point after stimulation. This plot is based on PIV analysis, where the vector components in the vector field are interpreted as cells in the cell sheet. The order of the graphs A to D is the order the images were taken in. The 5637 cells migrate in a mix of single cell- and collective migration. All the graphs, A-D, shows tendencies of both collective migration and single cell migration, as well as both fast and slow-moving migration.

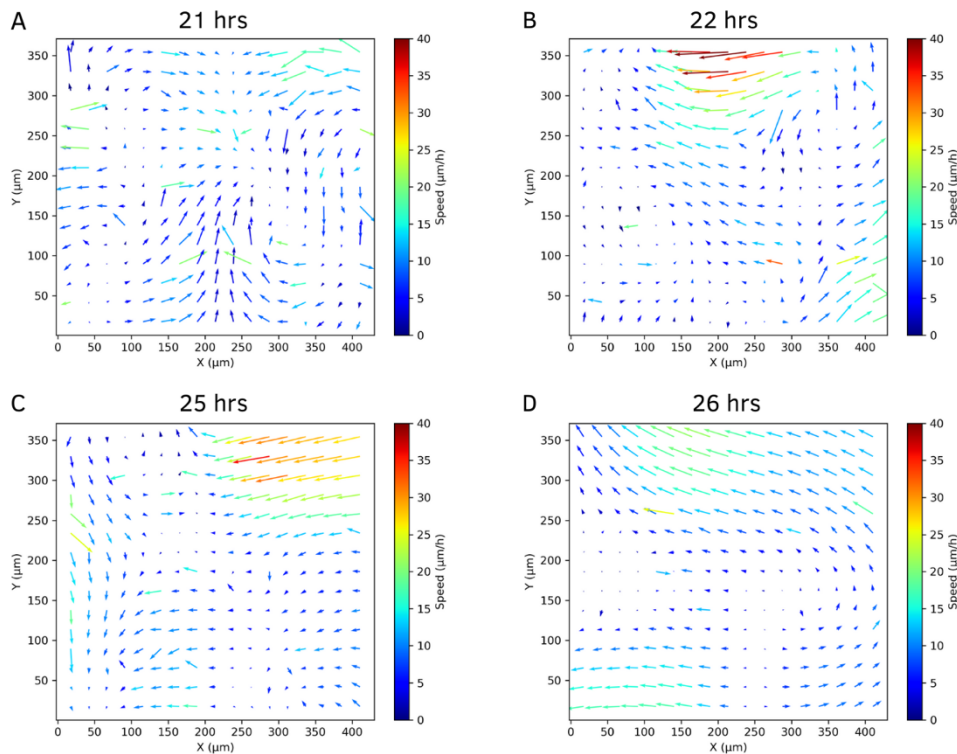


Figure 14: PIV graph of cell sheet migration of T24. The migration pattern of the cells is illustrated as arrows, to show the direction of cell movement at a given time point after stimulation. This plot is based on PIV analysis, where the vector components in the vector field are interpreted as cells in the cell sheet. The order of the graphs A to D is the order the images were taken in. The T24 cell line migrated as single cells as shown in A, single cells do not maintain cell-to-cell interaction, and migrate alone, in a disordinate pattern.

3.2 Traction forces impact on cell migration

Cancer cells were seeded onto collagen IV-coated polyacrylamide gels to detect traction forces on the gels, caused by the migrating cells, using a widefield microscope. We acquired z-stacks on the samples over time, using a fluorescence channel for detection of the fluorescent beads within the gels and a phase contrast channel for visualizing the cells. The cells were starved for a week to initiate the quiescent state. Before re-stimulation, images of starved cells were acquired, since previous studies in keratinocytes had shown that amplification of traction forces grew exponentially after adding serum. After the serum-containing medium was added to the cells, images were acquired over a period of 30 hrs to detect forces on the gels.

Figure 15 shows the variety in amplification of traction forces for the three cell lines. The traction magnitude, measured in pascal (Pa), from zero to 30 hrs after stimulation is shown. There is an immediate amplification of forces shown for all cell lines studied, and the traction

magnitude subsequently decreases and become stabilized, similar to observations in keratinocytes done by Lång, 2021. The 5637 and T24 cell lines show a higher amplification compared to SW780. However, T24 has the highest intensity of traction magnitude overall. After approximately 7-8 hrs of image acquisition, the forces instantly decrease and become stabilized. Similar to T24, 5637 had an intense amplification and a gradual decrease in traction magnitude. Finally, the SW780 cell line was the least intense, but same as T24 the forces decrease quickly and even out. Furthermore, on the bases of what was described in section 1.2.1, the cancer cells behaved similarly to keratinocytes, when the cells start migrating and dividing, the forces on substrates decline.

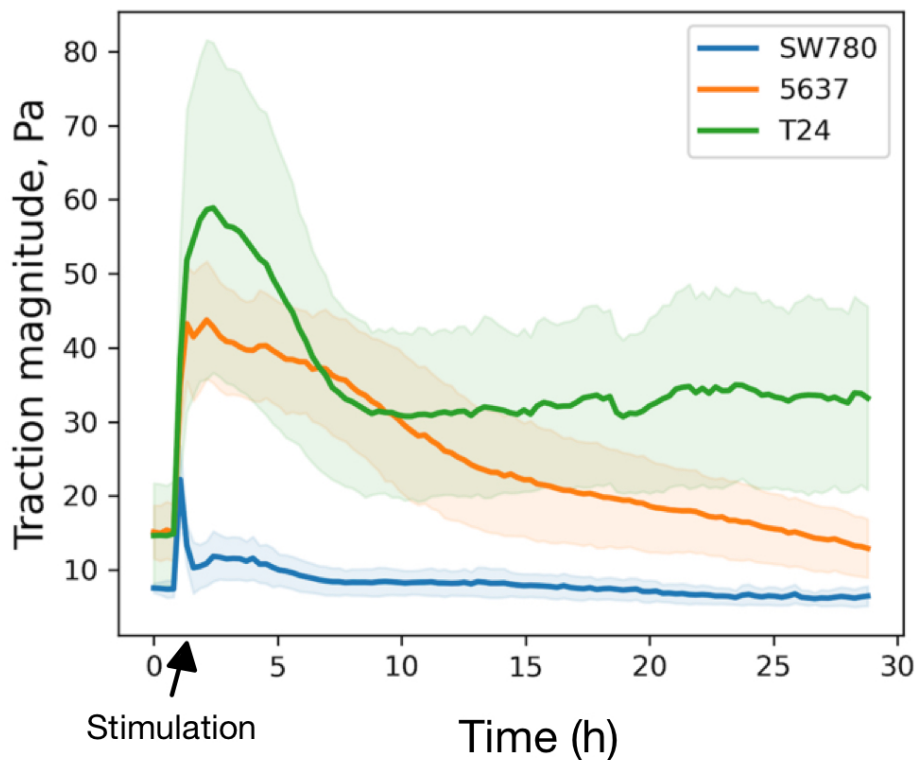


Figure 15: Measurements of the traction forces in the cell lines SW780 (blue), 5637 (orange), and T24 (green) over a 30 hrs period. The mean values are shown as the dark lines, while the areas of a lighter colors are the standard deviations. The traction forces are measured in Pascal.

3.3 Immunofluorescence (IF) staining

During the TFM experiment, a flower-like structure appeared in the SW780 cell line approximately 10 hrs after re-stimulation with FBS (figure 16). An IF experiment was performed to examine if the cells in these structures contained stem cell and/or mitotic markers. The antibodies used were raised against human SOX2 and Ki67. SOX2 is an important transcription factor for stem cells, and Ki67 is a marker for cell division

(proliferating cells). It was also added reagents to visualize the actin networks (Phalloidin 488) and cell nuclei (DAPI). The experiment was performed on the SW780 and T24 cell lines, where the cells were seeded into two Petri dishes for each cell line (four Petri dishes in total) and then starved for a week. One petri dish for each cell line was then stimulated 24 hrs before fixation and IF staining. Cells in the other two dishes were not stimulated before fixation and staining. IF staining was then analyzed using confocal microscopy. The experiment was run twice. The first time most of the cells detached from the coverslips, which had not been coated with collagen IV. The second time, coverslips were coated to avoid the cells from detaching, however, this was not successful and most of the cells detached once more. Hence, there was no result from this experiment.

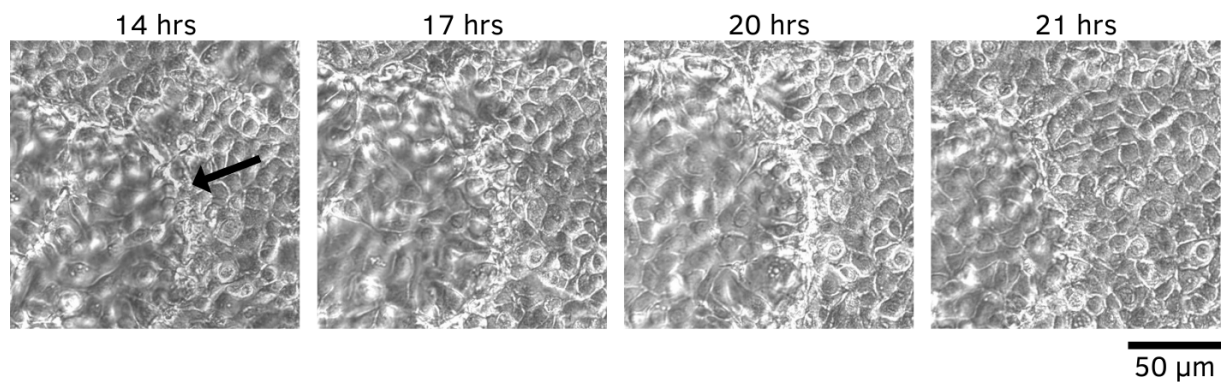


Figure 16: f lower-like structure appearance in the SW780 cell line with density of 25.000 cells/well. The structure appeared after approximately 10 hrs of imaging and disappear after approximately 21 hrs. The structure appears in the left corner of the images, however, there were several structures like this one seen in different places of the well. The images are listed in chronological order, where the image to the left is taken right before the structure started appearing, and the image to the right shows when the image had vanished.

4 Discussion

This study aimed to investigate the migration pattern and physical forces in cancer cell lines originating from urinary bladder cancer patients. Further, we wanted to see if the same migration pattern found in monolayers of quiescent human keratinocytes was detectable in other types of cells. Our results show that after re-stimulating quiescent bladder cancer cells, all three cell lines appear to have an increase in migration speed. They also showed an immediate amplification of traction forces after re-stimulation.

4.1 Behavior of urinary bladder cancer cell lines

Live cell imaging was the method used to analyze cell migration in this study. Tracking of both not starved cells and starved cells, followed by re-stimulation provided us with an understanding of the migration pattern in these cancer cell lines. The study shows that the cancer cells behave in a similar way as keratinocytes, considering the immediate burst of traction forces after re-stimulation, followed by a decrease of traction forces once the cells start to migrate. Data shows that the migration and traction forces follow the same pattern, however, the cancer cells do not have as strong of a reaction as the keratinocytes, as well as the results are not as long-lasting. In addition, the cancer cells start to migrate shortly after re-stimulation, whereas keratinocytes take longer time to exit quiescence and start migrating. One reason why the cancer cells have a less distinct, and shorter-lasting reaction, might be because these cells do not bind as firmly to each other and the substrate as keratinocytes. Another possible cause could be that cancer cell lines might be more heterogenic than the keratinocytes.

Both the graphs (Appendix C) and time-lapse videos of the cell migration show that in the wells with a higher density of cells, the cells showed a vibrating migration pattern rather than moving far, which could be due to limited space to move. Also, the cells seem to easily establish cell-to-cell interaction with neighboring cells and initiate collective migration, coordinately within the group. In addition, the cells migrating collectively were mostly circulating around the same area rather than migrating at longer distances. While in wells where there are fewer cells, the single cells migrated much faster and easier than groups of cells. Furthermore, we observed that single cells could move between groups of cells (changing neighbors), this was observed mostly in the cell lines T24 and 5637 with asynchronously growing cells. The complementary data (graphs) showing migration of starved and re-stimulated cells are shown in Appendix D.

The time lapse videos show different patterns when it comes to collective- and single-cell migration. We observed that all the cell lines had different patterns; T24 showed migration as single cells, SW780 showed a pattern of collective migration and 5637 had a partially collective migration, as the cells moved together but not in one particular direction and showed movements reminding of contractions. In figure 11 B, the graph of the re-stimulated cells shows that the cell lines T24 and 5637 have a slow and steady increase in migration. The cell line

SW780, however, shows a rapid increase before it slows down. There is a possibility that this is due to the SW780 being the only cell line with a distinct collective migration.

4.2 Measured traction forces

TFM was performed in order to map the physical forces of cancer cells that contribute to cell motility. The results show a similar reaction in all the cell lines, they all exhibit an evident boost of forces immediately after stimulation, in the same way as for keratinocytes. The quantity of forces, however, is distinct for the different cell lines. The cell line with the greatest amplification of forces is T24. On the other hand, the SW780 had a significantly lower increase of traction forces. Finally, 5637 had an increase in forces that was intermediate compared to the other two cell lines. There is a possibility that this boost of forces can be related to the migration pattern, as the cell line with single-cell migration (T24) has the highest peak and the cell line with the distinct collective migration (SW780) has the least evident peak. However, this should be studied further, and the experiment should be repeated. The keratinocytes show a huge amplification of forces and start migrating collectively many hours after stimulation.

Graphs of cell migration (see figure 11B) and traction forces (see figure 15) indicate that these features may be connected. As mentioned, T24 has the highest amplification of traction force overall but is also the one with the least migration average speed over time. The same pattern of connection applies to 5637 and SW780. SW780 had the least intensity of traction forces, but the most rapid increase of migration average speed in the early stage after re-stimulation. This may indicate that the traction forces have an impact on the migration speed.

4.3 Comparison of physical forces in cell sheets of urinary bladder cancer cells and keratinocytes

As stated in section 4.1, we can see from the results that the bladder cancer cells are showing a pattern of physical forces much like the one seen in keratinocytes. Having said that, there are still some differences causing the cancer cells to have a reaction of a smaller magnitude and not as long-lasting. One factor may be that keratinocytes have a better attachment to both the substrate and neighboring cells. The cancer cells seemed to be more independent leading to fewer interactions with the surrounding cells and substrate.

An epithelial-mesenchymal transition (EMT) may also be a factor affecting these cells. This process may lead to the epithelial cells (of the urinary bladder) expressing a mesenchymal cell phenotype, which can include increased migration capacity (Kalluri, 2009). The transition to a mesenchymal cell phenotype also participates in making the cancer cells more independent of surrounding cells. As the T24 cell line is the only cell line with clear single cell migration, and also the cell line that is the most invasive (Appendix E), these cells may be affected by a transition like the EMT.

4.4 Using immunofluorescence to investigate possible stem cell markers

A flower-like structure was observed in SW780 cell sheets during the TFM experiment, and confocal microscopy was performed to investigate the content of these structures. It was performed two repetitive experiments of IF staining and analysis by confocal microscopy, since the first experiment was unsuccessful due to not enough cells remaining in the samples. Hence, the results became unsatisfactory. Unfortunately, the second experiment was debilitated, all cells were also washed away from the coverslips during fixation or washing with PBS between steps (section 2.4.2).

In comparison to keratinocytes, it seems like urinary bladder cancer cells do not effortlessly bind to either substrate or neighboring cells. Hence it is a possible reason for an unsuccessful experiment with the thought that urinary bladder cancer cells are no longer behaving as epidermal cells. This may indicate the experiment was not suitable for these types of cells. Other possible sources of error can be that cell lines, in general, might change their characteristics if they are kept in culture and passaged over an extended period of time. Additionally, cells were cultured in much larger growth area for IF experiments, compared to cell migration experiments. This could affect the quality of the cells and even the cell's ability of attach to the surface.

5 Conclusion

The purpose of this study was to map the physical forces and dynamics of cancer cells isolated from urinary bladder cancers. Serum deprivation of cells and subsequent re-stimulation with serum-containing medium led to activation of increased cell motility. We cannot conclude that

all the cell lines have the exact same patterns of forces, but we do see both similar patterns among the different cancer cell lines, as well as patterns close to what has been discovered in keratinocytes. This common pattern shows a rapid increase of traction forces immediately after re-stimulation, in addition to a visible increase in migration following the amplification of forces. In conclusion, we see that starving and re-stimulating cells give a reaction of increased traction forces and migration. In addition, we cannot conclude with a common pattern when it comes to collective and single-cell migration, as all the cell lines exhibited different patterns.

6 Future perspectives

To further investigate and obtain a deeper understanding of the physical forces of cancer cells, and other cell types as well, we should perform multiple experiments. To begin with, we would like to repeat the traction force microscopy and live-cell imaging experiments on the urinary bladder cancer cell lines. These were only executed once, so it would be good to see if the results shown in this thesis could be verified. Further, the cells had been in culture for a while when some of the experiments were done, including the IF experiments. This may have an impact on the results; hence, we should try to do the experiments shortly after thawing the cells.

This project was executed to determine whether a similar mechanism as the one found in keratinocytes also was present in the urinary bladder cell lines. It would also be interesting to perform live cell imaging and traction force microscopy experiments on other cell types, including both other types of cancer cell lines and completely different cell types, like leukocytes (white blood cells). Not to mention, we could do an examination of the IF staining experiment with other types of cells. We should compare our cell lines with other cell types and investigate if our experiment was unsuccessful due to the practical execution or suitability of the cells in this experiment. Additionally, further research concerning the flower-like structures in the SW780 cell line would be interesting to investigate. As the fixation and IF staining was unsuccessful, expressing fluorescently labeled proteins in the cells (stable cell lines) to study live cells can be a potential future experiment.

References

- Alberts, B., Hopkin, K., Johnson, A., Morgan, D., Raff, M., Roberts, K., & Walter, P. (2019). *Essential Cell Biology 5th edition*. New York, NY: W. W. Norton & Company, Inc.
- Bauer, A., Prechova, M., Fischer, L., Thievensen, I., Gregor, M., & Fabry, B. (2021). pyTFM: A tool for traction force and monolayer stress microscopy. *PLoS Comput Biol*, 17(6), e1008364. <https://doi.org/10.1371/journal.pcbi.1008364>
- Bubenik, J., Baresova, M., Viklicky, V., Jakoubkova, J., Sainerova, H., & Donner, J. (1973). Established cell line of urinary bladder carcinoma (T24) containing tumour-specific antigen. *Int J Cancer*, 11(3), 765-773. <https://doi.org/10.1002/ijc.2910110327>
- Cooper, G. M. (2000). *The Cell: A Molecular Approach, 2nd ed*. Washington D.C: Sinauer Associates Inc.
- DeGeorge, K. C., Holt, H. R., & Hodges, S. C. (2017). Bladder Cancer: Diagnosis and Treatment. *Am Fam Physician*, 96(8), 507-514. <https://www.ncbi.nlm.nih.gov/pubmed/29094888>
- Desai, R. A., Gopal, S. B., Chen, S., & Chen, C. S. (2013). Contact inhibition of locomotion probabilities drive solitary versus collective cell migration. *J R Soc Interface*, 10(88), 20130717. <https://doi.org/10.1098/rsif.2013.0717>
- Fiore, A., Ribeiro, P. F., & Bruni-Cardoso, A. (2018). Sleeping Beauty and the Microenvironment Enchantment: Microenvironmental Regulation of the Proliferation-Quiescence Decision in Normal Tissues and in Cancer Development. *Front Cell Dev Biol*, 6, 59. <https://doi.org/10.3389/fcell.2018.00059>
- Frade, J. M., & Ovejero-Benito, M. C. (2015). Neuronal cell cycle: the neuron itself and its circumstances. *Cell Cycle*, 14(5), 712-720. <https://doi.org/10.1080/15384101.2015.1004937>
- Friedl, P., & Gilmour, D. (2009). Collective cell migration in morphogenesis, regeneration and cancer. *Nat Rev Mol Cell Biol*, 10(7), 445-457. <https://doi.org/10.1038/nrm2720>
- Gregers, T. F. (2020, 01 20). *Store Norske Leksikon*. Hentet fra snl.no: <https://snl.no/celle>
- Grendler, J., Lowgren, S., Mills, M., & Losick, V. P. (2019). Wound-induced polyploidization is driven by Myc and supports tissue repair in the presence of DNA damage. *Development*, 146(15). <https://doi.org/10.1242/dev.173005>
- Holck, P. (2021, 02 10). *Store medisinske leksikon*. Hentet fra sml.snl.no: <https://sml.snl.no/urinblaeren>
- Joshi, P., & Lee, M. Y. (2015). High Content Imaging (HCI) on Miniaturized Three-Dimensional (3D) Cell Cultures. *Biosensors (Basel)*, 5(4), 768-790. <https://doi.org/10.3390/bios5040768>
- Kalluri, R., & Weinberg, R. A. (2009). The basics of epithelial-mesenchymal transition. *J Clin Invest*, 119(6), 1420-1428. <https://doi.org/10.1172/JCI39104>
- Kan, A., & Hodgkin, P. D. (2014). Mechanisms of cell division as regulators of acute immune response. *Syst Synth Biol*, 8(3), 215-221.
- Kang, M. (2018). *Bladder Cancer*. Seoul, South Korea: Academic Press.
- Lång, E., Pedersen, C., Lång, A., Blicher, P., Klungland, A., Carlson, A., & Bøe, S. O. (2021). Mechanical coupling of supracellular stress amplification and tissue fluidization during exit from quiescence. *BioRxiv*.
- Lång, E., Polec, A., Lång, A., Valk, M., Blicher, P., Rowe, A. D., Tonseth, K. A., Jackson, C. J., Utheim, T. P., Janssen, L. M. C., Eriksson, J., & Bøe, S. O. (2018). Coordinated collective migration and asymmetric cell division in confluent human keratinocytes without wounding. *Nat Commun*, 9(1), 3665. <https://doi.org/10.1038/s41467-018-05578-7>

- Lekka, M., Gnanachandran, K., Kubiak, A., Zielinski, T., & Zemla, J. (2021). Traction force microscopy - Measuring the forces exerted by cells. *Micron*, 150, 103138. <https://doi.org/10.1016/j.micron.2021.103138>
- Mak, M., Spill, F., Kamm, R. D., & Zaman, M. H. (2016). Single-Cell Migration in Complex Microenvironments: Mechanics and Signaling Dynamics. *J Biomech Eng*, 138(2), 021004. <https://doi.org/10.1115/1.4032188>
- Marescal, O., & Cheeseman, I. M. (2020). Cellular Mechanisms and Regulation of Quiescence. *Dev Cell*, 55(3), 259-271. <https://doi.org/10.1016/j.devcel.2020.09.029>
- Masters, J. R., Hepburn, P. J., Walker, L., Highman, W. J., Trejdosiewicz, L. K., Povey, S., Parkar, M., Hill, B. T., Riddle, P. R., & Franks, L. M. (1986). Tissue culture model of transitional cell carcinoma: characterization of twenty-two human urothelial cell lines. *Cancer Res*, 46(7), 3630-3636. <https://www.ncbi.nlm.nih.gov/pubmed/3708594>
- McIntosh, J. R. (2016). Mitosis. *Cold Spring Harb Perspect Biol*, 8(9). <https://doi.org/10.1101/cshperspect.a023218>
- Meisslitzer-Ruppitsch, C., Rohrl, C., Neumuller, J., Pavelka, M., & Ellinger, A. (2009). Photooxidation technology for correlated light and electron microscopy. *J Microsc*, 235(3), 322-335. <https://doi.org/10.1111/j.1365-2818.2009.03220.x>
- Michaud, D. S., Spiegelman, D., Clinton, S. K., Rimm, E. B., Curhan, G. C., Willett, W. C., & Giovannucci, E. L. (1999). Fluid intake and the risk of bladder cancer in men. *N Engl J Med*, 340(18), 1390-1397. <https://doi.org/10.1056/NEJM199905063401803>
- Mohammad, R. M., Muqbil, I., Lowe, L., Yedjou, C., Hsu, H. Y., Lin, L. T., Siegelin, M. D., Fimognari, C., Kumar, N. B., Dou, Q. P., Yang, H., Samadi, A. K., Russo, G. L., Spagnuolo, C., Ray, S. K., Chakrabarti, M., Morre, J. D., Coley, H. M., Honoki, K., . . . Azmi, A. S. (2015). Broad targeting of resistance to apoptosis in cancer. *Semin Cancer Biol*, 35 Suppl, S78-S103. <https://doi.org/10.1016/j.semcancer.2015.03.001>
- Molecular Devices. (n.d.). *Molecular Devices*. Retrieved from ImageXpress Micro Confocal High-Content Imaging System : https://www.moleculardevices.com/products/cellular-imaging-systems/high-content-imaging/imageexpress-micro-confocal?cmp=7014u000001t0pGAAQ&utm_source=AdWords&utm_medium=cpc&utm_campaign=IMG-Brand_Regional_NOFI&utm_adgroup=%7Badgroup%7D&utm_location=1010826
- Nwaneshiudu, A., Kuschal, C., Sakamoto, F. H., Anderson, R. R., Schwarzenberger, K., & Young, R. C. (2012). Introduction to confocal microscopy. *J Invest Dermatol*, 132(12), e3. <https://doi.org/10.1038/jid.2012.429>
- Pandya, P., Orgaz, J. L., & Sanz-Moreno, V. (2017). Actomyosin contractility and collective migration: may the force be with you. *Curr Opin Cell Biol*, 48, 87-96. <https://doi.org/10.1016/j.ceb.2017.06.006>
- Pastar, I., Stojadinovic, O., Yin, N. C., Ramirez, H., Nusbaum, A. G., Sawaya, A., Patel, S. B., Khalid, L., Isseroff, R. R., & Tomic-Canic, M. (2014). Epithelialization in Wound Healing: A Comprehensive Review. *Adv Wound Care (New Rochelle)*, 3(7), 445-464. <https://doi.org/10.1089/wound.2013.0473>
- Recasens, A., & Munoz, L. (2019). Targeting Cancer Cell Dormancy. *Trends Pharmacol Sci*, 40(2), 128-141. <https://doi.org/10.1016/j.tips.2018.12.004>
- Ridley, A. J., Schwartz, M. A., Burridge, K., Firtel, R. A., Ginsberg, M. H., Borisy, G., Parsons, J. T., & Horwitz, A. R. (2003). Cell migration: integrating signals from front to back. *Science*, 302(5651), 1704-1709. <https://doi.org/10.1126/science.1092053>

- Saginala, K., Barsouk, A., Aluru, J. S., Rawla, P., Padala, S. A., & Barsouk, A. (2020). Epidemiology of Bladder Cancer. *Med Sci (Basel)*, 8(1). <https://doi.org/10.3390/medsci8010015>
- Sanderson, M. J., Smith, I., Parker, I., & Bootman, M. D. (2014). Fluorescence microscopy. *Cold Spring Harb Protoc*, 2014(10), pdb top071795. <https://doi.org/10.1101/pdb.top071795>
- Sanli, O., Dobruch, J., Knowles, M. A., Burger, M., Alemozaffar, M., Nielsen, M. E., & Lotan, Y. (2017). Bladder cancer. *Nat Rev Dis Primers*, 3, 17022. <https://doi.org/10.1038/nrdp.2017.22>
- Scarpa, E., & Mayor, R. (2016). Collective cell migration in development. *J Cell Biol*, 212(2), 143-155. <https://doi.org/10.1083/jcb.201508047>
- Schouw, H. M., Huisman, L. A., Janssen, Y. F., Slart, R., Borra, R. J. H., Willemsen, A. T. M., Brouwers, A. H., van Dijk, J. M., Dierckx, R. A., van Dam, G. M., Szymanski, W., Boersma, H. H., & Kruijff, S. (2021). Targeted optical fluorescence imaging: a meta-narrative review and future perspectives. *Eur J Nucl Med Mol Imaging*, 48(13), 4272-4292. <https://doi.org/10.1007/s00259-021-05504-y>
- Schwarz, U. S., & Soine, J. R. (2015). Traction force microscopy on soft elastic substrates: A guide to recent computational advances. *Biochim Biophys Acta*, 1853(11 Pt B), 3095-3104. <https://doi.org/10.1016/j.bbamcr.2015.05.028>
- Serra-Picamal, X., Conte, V., Sunyer, R., Munoz, J. J., & Trepast, X. (2015). Mapping Forces and Kinematics during Collective cell migration. I *Biophysical Methods in Cell Biology* (ss. 309-330). Cambridge, Massachusetts: Academic Press.
- Shermadou, E. S., Rahman, S., & Leslie, S. W. (2022). Anatomy, Abdomen and Pelvis, Bladder. In *StatPearls*. <https://www.ncbi.nlm.nih.gov/pubmed/30285360>
- Te Boekhorst, V., Preziosi, L., & Friedl, P. (2016). Plasticity of Cell Migration In Vivo and In Silico. *Annu Rev Cell Dev Biol*, 32, 491-526. <https://doi.org/10.1146/annurev-cellbio-111315-125201>
- Urology Care Foundation. (n.d.). *Urology Care Foundation*. Hentet fra Urologyhealth.org: <https://www.urologyhealth.org/urology-a-z/i/interstitial-cystitis>
- Vallo, S., Michaelis, M., Rothweiler, F., Bartsch, G., Gust, K. M., Limbart, D. M., Rodel, F., Wezel, F., Haferkamp, A., & Cinatl, J., Jr. (2015). Drug-Resistant Urothelial Cancer Cell Lines Display Diverse Sensitivity Profiles to Potential Second-Line Therapeutics. *Transl Oncol*, 8(3), 210-216. <https://doi.org/10.1016/j.tranon.2015.04.002>
- Wessels, J. T., Pliquett, U., & Wouters, F. S. (2012). Light-emitting diodes in modern microscopy--from David to Goliath? *Cytometry A*, 81(3), 188-197. <https://doi.org/10.1002/cyto.a.22023>
- Zhou, J., Kelsey, K. T., Smith, S., Giovannucci, E., & Michaud, D. S. (2015). Lower Urinary Tract Symptoms and Risk of Bladder Cancer in Men: Results From the Health Professionals Follow-up Study. *Urology*, 85(6), 1312-1318. <https://doi.org/10.1016/j.urology.2015.02.024>

Appendix A: Recipe for PBS buffer

PBS (Phosphate-buffered Saline)

NaCl: 137 mM

KCl: 2.7 mM

Na₂HPO₄: 10 mM

KH₂PO₄: 1.8 mM

Appendix B: Python-based scripts

B.1: Script for sorting data – file_sorting.py

```
import os
import shutil
import sys

'''
This program sorts files from ImageXpress 96-well time laps experiments into folders where each folder represents all timepoints from one
well. To use the program, place all TimePoint folders into the folder called "test". The "Wells"-folder containing all of the 96-well subfolders
will be generated automatically.
'''

Wells = "C:\\Users\\huygens\\Emma_Linda\\Exp2_stimulated_edge\\Wells\\" #Dont change \\Wells\\

os.makedirs(Wells)

#make new folder names
folder_name = ["A01", "A02", "A03", "A04", "A05", "A06", "A07", "A08", "A09", "A10", "A11", "A12", "B01", "B02", "B03", "B04", "B05", "B06",
"B07", "B08", "B09", "B10", "B11", "B12", "C01", "C02", "C03", "C04", "C05", "C06", "C07", "C08", "C09", "C10", "C11", "C12", "D01", "D02",
"D03", "D04", "D05", "D06", "D07", "D08", "D09", "D10", "D11", "D12", "E01", "E02", "E03", "E04", "E05", "E06", "E07", "E08", "E09", "E10",
"E11", "E12", "F01", "F02", "F03", "F04", "F05", "F06", "F07", "F08", "F09", "F10", "F11", "F12", "G01", "G02", "G03", "G04", "G05", "G06",
"G07", "G08", "G09", "G10", "G11", "G12", "H01", "H02", "H03", "H04", "H05", "H06", "H07", "H08", "H09", "H10", "H11", "H12"]

#iterate through the files in your directory
for x in range(0, len(folder_name)):
    if not os.path.exists(Wells+folder_name[x]):
        os.makedirs(Wells+folder_name[x])

for Timepoints in range(0, 101): #number of timepoints (must be exact)
    path = "C:\\Users\\huygens\\Emma_Linda\\Exp2_stimulated_edge\\TimePoint_"+str(Timepoints+1)+"\\" #Dont change
    \\TimePoint_"+str(Timepoints+1)+"\\"
    time = "Timepoint_"+"%.3d" % (Timepoints + 1)

#make a list of all the files in a directory and store it in the variable names
#Note that the command os.listdir dose not work since the items wil not be iterable
names = []
for subdir, dirs, files in os.walk(path):
    for file in files:
        names.append(os.path.join(file))

for files in names:
    if "A01" in files and not os.path.exists(Wells+"A01/"+time+"_"+files):
        shutil.move(path+files, Wells+"A01/"+time+"_"+files)
    if "A02" in files and not os.path.exists(Wells+"A02/"+time+"_"+files):
        shutil.move(path+files, Wells+"A02/"+time+"_"+files)
    if "A03" in files and not os.path.exists(Wells+"A03/"+time+"_"+files):
        shutil.move(path+files, Wells+"A03/"+time+"_"+files)
    if "A04" in files and not os.path.exists(Wells+"A04/"+time+"_"+files):
        shutil.move(path+files, Wells+"A04/"+time+"_"+files)
    if "A05" in files and not os.path.exists(Wells+"A05/"+time+"_"+files):
        shutil.move(path+files, Wells+"A05/"+time+"_"+files)
    if "A06" in files and not os.path.exists(Wells+"A06/"+time+"_"+files):
        shutil.move(path+files, Wells+"A06/"+time+"_"+files)
    if "A07" in files and not os.path.exists(Wells+"A07/"+time+"_"+files):
        shutil.move(path+files, Wells+"A07/"+time+"_"+files)
    if "A08" in files and not os.path.exists(Wells+"A08/"+time+"_"+files):
        shutil.move(path+files, Wells+"A08/"+time+"_"+files)
    if "A09" in files and not os.path.exists(Wells+"A09/"+time+"_"+files):
        shutil.move(path+files, Wells+"A09/"+time+"_"+files)
    if "A10" in files and not os.path.exists(Wells+"A10/"+time+"_"+files):
        shutil.move(path+files, Wells+"A10/"+time+"_"+files)
    if "A11" in files and not os.path.exists(Wells+"A11/"+time+"_"+files):
        shutil.move(path+files, Wells+"A11/"+time+"_"+files)
```



```

if "G07" in files and not os.path.exists(Wells + "G07/" + time + "_" + files):
    shutil.move(path + files, Wells + "G07/" + time + "_" + files)
if "G08" in files and not os.path.exists(Wells + "G08/" + time + "_" + files):
    shutil.move(path + files, Wells + "G08/" + time + "_" + files)
if "G09" in files and not os.path.exists(Wells + "G09/" + time + "_" + files):
    shutil.move(path + files, Wells + "G09/" + time + "_" + files)
if "G10" in files and not os.path.exists(Wells + "G10/" + time + "_" + files):
    shutil.move(path + files, Wells + "G10/" + time + "_" + files)
if "G11" in files and not os.path.exists(Wells + "G11/" + time + "_" + files):
    shutil.move(path + files, Wells + "G11/" + time + "_" + files)
if "G12" in files and not os.path.exists(Wells + "G12/" + time + "_" + files):
    shutil.move(path + files, Wells + "G12/" + time + "_" + files)

if "H01" in files and not os.path.exists(Wells + "H01/" + time + "_" + files):
    shutil.move(path + files, Wells + "H01/" + time + "_" + files)
if "H02" in files and not os.path.exists(Wells + "H02/" + time + "_" + files):
    shutil.move(path + files, Wells + "H02/" + time + "_" + files)
if "H03" in files and not os.path.exists(Wells + "H03/" + time + "_" + files):
    shutil.move(path + files, Wells + "H03/" + time + "_" + files)
if "H04" in files and not os.path.exists(Wells + "H04/" + time + "_" + files):
    shutil.move(path + files, Wells + "H04/" + time + "_" + files)
if "H05" in files and not os.path.exists(Wells + "H05/" + time + "_" + files):
    shutil.move(path + files, Wells + "H05/" + time + "_" + files)
if "H06" in files and not os.path.exists(Wells + "H06/" + time + "_" + files):
    shutil.move(path + files, Wells + "H06/" + time + "_" + files)
if "H07" in files and not os.path.exists(Wells + "H07/" + time + "_" + files):
    shutil.move(path + files, Wells + "H07/" + time + "_" + files)
if "H08" in files and not os.path.exists(Wells + "H08/" + time + "_" + files):
    shutil.move(path + files, Wells + "H08/" + time + "_" + files)
if "H09" in files and not os.path.exists(Wells + "H09/" + time + "_" + files):
    shutil.move(path + files, Wells + "H09/" + time + "_" + files)
if "H10" in files and not os.path.exists(Wells + "H10/" + time + "_" + files):
    shutil.move(path + files, Wells + "H10/" + time + "_" + files)
if "H11" in files and not os.path.exists(Wells + "H11/" + time + "_" + files):
    shutil.move(path + files, Wells + "H11/" + time + "_" + files)
if "H12" in files and not os.path.exists(Wells + "H12/" + time + "_" + files):
    shutil.move(path + files, Wells + "H12/" + time + "_" + files)

print("...done with " + files)

#os.rmdir(path)

```

B.2: Script for plotting TrackMate data

```

import matplotlib.pyplot as plt
import pandas as pd
import numpy as np
import os
import openpyxl as openpyxl

def extract_file_names_from_directory(directory):
    file_names = []
    for subdir, dirs, files in os.walk(directory):
        for file in files:
            file_names.append(os.path.join(file))
    return file_names

def average_single_site(file):
    df = pd.read_csv(path + file, usecols=["SPEED", "EDGE_TIME"], low_memory=False)
    column = df["EDGE_TIME"]
    column = column[3:].to_numpy(dtype=float)
    range = np.arange(0.5, column.max() + 1, 1)
    average_list = []
    for i in range:
        time_point = df.loc[df['EDGE_TIME'] == str(i)]
        speed = time_point["SPEED"]
        speed = speed[3:].to_numpy(dtype=float)

```

```

    average = np.average(speed)
    average_list.append(average)
return average_list

def get_column_list(list, ark):
    column_list = []
    for name in list:
        for i in range(0, ark.max_column):
            if name in str(ark.cell(row = 1, column = i + 1).value):
                column_list.append(i+1)
    return(column_list)

def get_colun(column_number, ark):
    column=np.zeros(ark.max_row)
    for i in range(0, ark.max_row-2):
        column[i] = ark.cell(column = column_number, row = i +2).value
    return(column)

def get_row_average(column_list, ark, row_number):
    row_numbers = []
    for i in column_list:
        row_numbers.append(ark.cell(column = i, row = row_number).value)
    average = np.average((row_numbers))
    return(average)

def X_axis(interval, ark):
    X = np.zeros(ark.max_row)
    for i in range(0, ark.max_row):
        X[i] = (i*interval)/60
    return(X)

#Define the path where the files are stored. Note the use of double back_slash
path = "E:\\Linda_Emma\\Combine_Exp2_Exp4\\Stimulated\\"

# Get the file names
file_names = extract_file_names_from_directory(directory = path)

print(file_names)

List_of_data = []
header = []

for file in file_names:
    data=average_single_site(file)
    List_of_data.append(data)
    name = file[:-9]
    header.append(name)

#Create a dataframe with all the data
df = pd.DataFrame(data=List_of_data, index=header).T

# Save to Excel
df.to_excel('Data.xlsx', index=False, header=header)

#Plot data from excel file
wb = openpyxl.load_workbook("Data.xlsx", data_only=True)
ark = wb.active

# Put names of columns to be plotted here
# It is sufficient to use only part of the column index name (example well name "A01s1"), but it has to be specific for that column
plot_list = [{"A04_s1", "A04_s3", "A04_s4", "B04_s1", "B04_s3", "B04_s4"}, {"E04_s1", "E04_s2", "E04_s3", "E04_s4",
"F04_s1", "F04_s2", "F04_s3", "F04_s4"},
["C04_s1", "C04_s3", "C04_s4", "D04_s1", "D04_s3", "D04_s4"]]

# For each line in the graph put a label here
label_list = ["SW780", "5637", "T24"]

```

```

average_list = []
std_list = []

for group in plot_list:
    column_list=get_column_list(list=group, ark=ark)
    columns=[]
    for i in column_list:
        column=get_colun(column_number=i, ark=ark)
        columns.append(column)
    average=(np.average(columns, axis=0))*0.7018    #Multiply with pixelsize (µm/pixel)
    Average=(average/4)*60                        #Divide with time interval and multiply with 60 to get values in µm/h
    std=(np.std(columns, axis=0))*0.7018          #Multiply with pixelsize (µm/pixel)
    STD=(std/4)*60                                #Divide with time interval and multiply with 60 to get values in µm/h
    average_list.append(Average)
    std_list.append(STD)

x = X_axis(interval = 4, ark = ark)

fig, ax = plt.subplots(ncols=1, nrows=1, figsize = (8, 5))

for average, std, label in zip(average_list, std_list, label_list):
    plt.plot(x[1:-2], average[1:-2], alpha = 1, label=label)
    plt.fill_between(x[1:-2], average[1:-2]-std[1:-2], average[1:-2]+std[1:-2], alpha=0.4)

plt.legend(loc='upper left', bbox_to_anchor=(0.85, 1.00), prop={'size': 8})
plt.ylim(0, 80)
plt.xlabel("Time (h)", fontsize=14)
plt.ylabel("Average speed (µm/h)", fontsize=14)
#plt.title("Urinary bladder cells", fontsize=14)
plt.savefig("Combine_Exp2_Exp4_12500cells_stimulated_std.png", format='png', dpi=300)

plt.show()

```

B.3: Script for plotting Traction Forces

B.3.1 Macro_concatenate.ijm

– merging images of TFM from respective site, allegedly “starved, activate 1, activate 2 and trypsin” files become one time lapse per site.

n = 1

```

run("Bio-Formats Importer", "open=[F:/080322_MRC5/Reference(" + n + ").czi] color_mode=Composite open_files rois_import=[ROI manager] view=Hyperstack stack_order=XYCZT use_virtual_stack");
rename("s1");
roiManager("Select", 0);
run("Duplicate...", "duplicate");
run("Z Project...", "projection=[Max Intensity]");
selectWindow("s1-1");
close();
selectWindow("s1");
close();

run("Bio-Formats Importer", "open=[F:/080322_MRC5/Starved(" + n + ").czi] color_mode=Composite open_files rois_import=[ROI manager] view=Hyperstack stack_order=XYCZT use_virtual_stack");
rename("s2");
roiManager("Select", 0);
run("Duplicate...", "duplicate");
run("Z Project...", "projection=[Max Intensity] all");
selectWindow("s2-1");
close();
selectWindow("s2");
close();

run("Bio-Formats Importer", "open=[F:/080322_MRC5/Activated1(" + n + ").czi] color_mode=Composite open_files rois_import=[ROI manager] view=Hyperstack stack_order=XYCZT use_virtual_stack");

```

```

rename("s3");
roiManager("Select", 0);
run("Duplicate...", "duplicate");
run("Z Project...", "projection=[Max Intensity] all");
selectWindow("s3-1");
close();
selectWindow("s3");
close();

run("Bio-Formats Importer", "open=[F:/080322_MRC5/Activated2(" + n + ").czi] color_mode=Composite open_files rois_import=[ROI
manager] view=Hyperstack stack_order=XYCZT use_virtual_stack");
rename("s4");
roiManager("Select", 0);
run("Duplicate...", "duplicate");
run("Z Project...", "projection=[Max Intensity] all");
selectWindow("s4-1");
close();
selectWindow("s4");
close();

run("Bio-Formats Importer", "open=[F:/080322_MRC5/Activated3(" + n + ").czi] color_mode=Composite open_files rois_import=[ROI
manager] view=Hyperstack stack_order=XYCZT use_virtual_stack");
rename("s5");
roiManager("Select", 0);
run("Duplicate...", "duplicate");
run("Z Project...", "projection=[Max Intensity] all");
selectWindow("s5-1");
close();
selectWindow("s5");
close();

run("Concatenate...", " title=concat open image1=MAX_s1-1 image2=MAX_s2-1 image3=MAX_s3-1 image4=MAX_s4-1 image4=MAX_s5-1");
makeRectangle(0, 0, 1318, 1248);
run("Descriptor-based series registration (2d/3d + t)", "series_of_images=concat brightness_of=[Interactive ...]
approximate_size=[Interactive ...] type_of_detections=[Interactive ...] subpixel_localization=[3-dimensional quadratic fit]
transformation_model=[Rigid (2d)] number_of_neighbors=3 redundancy=1 significance=3 allowed_error_for_ransac=5
global_optimization=[All against first image (no global optimization)] range=5 choose_registration_channel=1 image=[Fuse and display]
interpolation=[Linear Interpolation]");
selectWindow("concat");
close();
selectWindow("registered concat");
saveAs("Tiff", "F:/080322_MRC5/Samples/Sample" + n + ".tif");
close();

```

B.3.2 Macro_TFM.ijm

- removes the "trypsin" image from the rest of the respective time lapse.

```

x=newArray(1,2,3,4,5,6,7,8,9,10,11,12,13,14,15,16,17,18,19,20,21,22,23,24,25,26,27,28,29,30,31,32,33,34,35,36,37,38,39,40,41,42,43,44,4
5,46,48)

for ( i=0 ; i < x.length; i++) {

    open("F:/080322_MRC5/Samples/Sample" + x[i] + ".tif");

    rename("image");
    run("Duplicate...", "duplicate channels=1");
    run("Duplicate...", "use");

    saveAs("Tiff", "F:/080322_MRC5/Data/Ref" + x[i] + ".tif");

    close();
    run("Duplicate...", "duplicate range=2-121 use");

    run("Image Sequence... ", "select=[F:/080322_MRC5/Data/AFM_Sample" + x[i] + "/] dir=[F:/080322_MRC5/Data/AFM_Sample" +
x[i] + "/] format=TIFF");

```

```

        close();
        close();
        selectWindow("image");
        run("Duplicate...", "duplicate channels=2 frames=2-121");

        run("Image Sequence... ", "select=[F:/080322_MRC5/PIV/Raw" + x[i] + "/" ] dir=[F:/080322_MRC5/PIV/Raw" + x[i] + "/" ]
format=TIFF");

        close();
        selectWindow("image");
        close();
    }

```

B.3.3 Traction3_Batch

- calculates the traction forces components. Bead displacements in time lapse are compared with the "trypsin / reference" image.

```

from pyTFM.TFM_functions import calculate_deformation, TFM_tractions, strain_energy_points, contractility
from pyTFM.plotting import show_quiver, plot_continuous_boundary_stresses
from pyTFM.stress_functions import lineTension
from pyTFM.grid_setup_solid_py import interpolation, prepare_forces, grid_setup, FEM_simulation, find_borders
from pyTFM.utilities_TFM import round_flexible
import numpy as np
import matplotlib.pyplot as plt
from scipy.ndimage.morphology import binary_fill_holes
import os
import pandas as pd
import scipy.ndimage
import numpy as np

def edges(m, edge):
    return m[edge:-edge, edge:-edge]

def extract_file_names_from_directory(directory):
    """This function takes in a directory and extract the file_names contained in it"""
    file_names = []
    for subdir, dirs, files in os.walk(directory):
        for file in files:
            file_names.append(os.path.join(subdir, file))
    return file_names

def get_data(n):
    path = "E:\\02052022_TFM_inhibitors\\Data\\AFM_Sample" + str(n) + "\\\" # Get the raw beads time series
    path_out_im = "E:\\02052022_TFM_inhibitors\\Data\\Movie" + str(n) + "\\\" # Store the output TFM map
    path_out_data = "E:\\02052022_TFM_inhibitors\\Data\\Data_Sample" + str(n) + "\\\" # Store the calculated data
    ref_image = "E:\\02052022_TFM_inhibitors\\Data\\Ref" + str(n) + ".tif" # Get the reference image

    names = extract_file_names_from_directory(path)

    tM_average_list = []
    tM_average_points = []

    ty_average_list = []
    ty_average_points = []

    u_average_list = []
    u_average_points = []

    k = 0
    for name in names:
        im_path1 = path + name
        im_path2 = ref_image

        u, v, mask_val, mask_std = calculate_deformation(im_path1, im_path2, window_size = 13, overlap = 8)
        # The unit of window size and overlap is pixels, so you need to adapt them according
        # to your pixel size

```



```

# plotting the deformation field
#fig1, ax = show_quiver(u, v, cbar_str="deformations\n[pixels]")# plotting

## calculating a traction forces

# important parameters:
ps1 = 0.65 # pixel size of the image of the beads
im1_shape = (1258, 1358) # dimensions of the image of the beads
ps2 = ps1 * np.mean(np.array(im1_shape) / np.array(u.shape)) # pixel size of of the deformation field
young = 4000 # Young's modulus of the substrate
sigma = 0.46 # Poisson's ratio of the substrate
h = 60 # height of the substrate in  $\mu\text{m}$ , "infinite" is also accepted

tx, ty = TFM_tractions(u, v, pixelsize1=ps1, pixelsize2=ps2, h=h, young=young, sigma=sigma)
tM = np.hypot(tx, ty)

tx = edges(tx, 10)
#resized_tx = scipy.ndimage.zoom(tx, 100. / 225)

ty = edges(ty, 10)
#resized_ty = scipy.ndimage.zoom(ty, 100. / 225)

tM = edges(tM, 10)
#resized_tM = scipy.ndimage.zoom(tM, 100. / 225)

im = plt.imshow(tM, vmin = 0, vmax=50, cmap = "jet", extent=[0, 866, 0, 814])

print("Min and max:")
print(tM.min(), tM.max())

bar = plt.colorbar(im)
bar.set_label("Traction Tx (Pa)")
plt.xlabel(" $\mu\text{m}$ ")
plt.ylabel(" $\mu\text{m}$ ")
plt.gca().set_aspect('equal', adjustable='box')
plt.savefig(path_out_im + "image_ty" + str(k))
plt.close()

k = k + 1
print("Done with image " + str(k) + " from Sample " + str(n))

tM_average = np.average(tM, axis=0)
tM_average_list.append(tM_average)

tM_average_point = np.average(Sanderson et al.)
tM_average_points.append(tM_average_point)

ty_average = np.average(ty, axis=0)
ty_average_list.append(ty_average)

ty_average_point = np.average(ty)
ty_average_points.append(ty_average_point)

u_average = np.average(u, axis=0)
u_average_list.append(u_average)

u_average_point = np.average(u)
u_average_points.append(u_average_point)

pd.DataFrame(tM_average_list).to_csv(path_out_data + "tM_list.csv", header=None, index=None)
pd.DataFrame(tM_average_points).to_csv(path_out_data + "tM_points.csv", header=None, index=None)

pd.DataFrame(ty_average_list).to_csv(path_out_data + "ty_list.csv", header=None, index=None)
pd.DataFrame(ty_average_points).to_csv(path_out_data + "ty_points.csv", header=None, index=None)

pd.DataFrame(u_average_list).to_csv(path_out_data + "u_list.csv", header=None, index=None)
pd.DataFrame(u_average_points).to_csv(path_out_data + "u_points.csv", header=None, index=None)

```

```

#sample_list = [3]
sample_list =
[1,2,3,4,5,6,7,8,9,10,11,12,13,14,15,16,17,18,19,20,21,22,23,24,25,26,27,28,29,30,31,32,33,34,35,36,37,38,39,40,41,42,43,44,45,46,47,48]
#sample_list = [25,26,27,28,29,30,31,32]

for n in sample_list:
    get_data(n)

```

B.3.4 Graph2

-Graph2 shows graphs for all data. If you enter data from several sites, the mean and standard deviation are calculated.

```

import pandas as pd
import matplotlib.pyplot as plt
import numpy as np

def moving_average(a, n=3):
    ret = np.cumsum(a, dtype=float)
    ret[n:] = ret[n:] - ret[:-n]
    return ret[n - 1:] / n

def plot(sample_list, data_type, label, color):

    sample_list = sample_list
    data_list= []
    for i in sample_list:
        data = pd.read_csv("F:\25042022_TFM_Inhibitors\Data\Data_Sample" + str(i) + "\\" + data_type + ".csv", header=None)
        #data = data.drop([4])
        #data = data.drop([251])
        data_list.append(data)
        print(data)
        print(str(i) + ": " + str(len(data)))

    average = np.average(data_list, axis=0)
    std = np.std(data_list, axis=0)

    average = np.ndarray.flatten(average)
    std = np.ndarray.flatten(std)

    x = np.arange(0, len(average))
    x = np.multiply(x, 16)
    x = np.divide(x, 60)

    a = plt.plot(x[:-7], average[:-7], "-", mfc = "None", lw=2, label = label, alpha=1, c = color)
    s = plt.fill_between(x[:-7], average[:-7] + std[:-7], average[:-7] - std[:-7], alpha = 0.1, color = color)
    return a, s

fig, ax = plt.subplots(figsize = (5, 4))
a0, s0 = plot([1, 5], "tM_points", "FBS", "C0")
#a1, s1 = plot([9, 10, 11, 12, 13, 14, 15, 16], "tM_points", "RO-3306 5µM", "C1")
#a2, s2 = plot([19, 20, 21,22,23,24], "tM_points", "RO-3306 10µM", "C2")
#a3, s3 = plot([33, 35, 37, 38, 39, 40], "tM_points", "SMIFH2", "C3")
a4, s4 = plot([41, 42, 43, 44, 45, 46, 47, 48], "tM_points", "EHT 1864", "C4")

#a1, s1 = plot([17, 18, 19, 20], "tM_points", "RO-3306 10µM well 1", "C1")
#a2, s2 = plot([21,22,23,24], "tM_points", "RO-3306 10µM well 2", "C2")#a, s = plot([21, 22, 23, 24], "tM_points", "8h", "C3")
#a3, s3 = plot([13, 14, 15, 16], "tM_points", "22h", "C4")
#a4, s4 = plot([25, 26, 27, 28, 29, 30, 31, 32], "tM_points", "29h", "C5")
#a5, s5 = plot([37, 38, 39, 40], "tM_points", "5h", "C6")
#a6, s6 = plot([41, 42, 43, 44], "tM_points", "2h", "C7")
#a7, a8 = plot([45, 46, 47, 48], "tM_points", "0h", "C8")

```

```

plt.ylim(0, 80)
plt.xlim(0, 30)
plt.legend()
plt.ylabel("Traction magnitude, Pa", fontsize=14)
plt.xlabel("Time (h)", fontsize=14)

plt.savefig("F:\\25042022_TFM_Inhibitors\\Graphs\\Fig 10 FBS + RO-3306 10µM well 2.png", dpi = 300)
plt.savefig(save + "LPA", dpi = 300)

plt.show()

```

B.4: Script for PIV-analysis of migration speed and direction – Quiver.py

```

import numpy as np
from openpiv import tools, validation, process, filters, scaling, pyprocess
from scipy.ndimage import rotate
import os
import openpyxl
import time
import matplotlib.pyplot as plt
import scipy.ndimage

def extract_file_names_from_directory(directory):
    """This function takes in a directory and extract the file_names contained in it"""
    file_names = []
    for subdir, dirs, files in os.walk(directory):
        for file in files:
            file_names.append(os.path.join(file))
    return file_names

def scale2(u, v, M, factor):
    u2 = np.multiply(u, factor)
    v2 = np.multiply(v, factor)
    M2 = np.multiply(M, factor)
    return u2, v2, M2

def PIV(frame_a, frame_b, window_size, overlap, search_area_size):
    frame_a = tools.imread(frame_a)
    frame_b = tools.imread(frame_b)
    u, v, sig2noise = process.extended_search_area_piv(frame_a.astype(np.int32), frame_b.astype(np.int32),
        window_size=window_size, overlap=overlap, search_area_size=search_area_size, sig2noise_method='peak2peak')
    x, y = process.get_coordinates( image_size=frame_a.shape, window_size=window_size, overlap=overlap)
    u, v, mask = validation.sig2noise_val( u, v, sig2noise, threshold = 1.5)
    u, v, mask = validation.global_val( u, v, (-10, 10), (-10, 10) )
    u, v = filters.replace_outliers( u, v, method='localmean', max_iter=10, kernel_size=4)
    # tools.save(x, y, u, v, mask, 'exp1_001.txt')
    # display_vector_field('exp1_001.txt', scale=1000, width=0.0025)
    M = np.hypot(u, v)
    print(M.min(), M.max())
    return x, y, u, v, M

path = "C:\\Users\\huygens\\PycharmProjects\\Migration\\Linda_Emma_20.05\\T24\\Exp2_T24_24000_C03\\Raw_data\\"
path_out = "C:\\Users\\huygens\\PycharmProjects\\Migration\\Linda_Emma_20.05\\T24\\out_T24\\"

names = extract_file_names_from_directory(path)
print(names)

k= 0
for frame_a, frame_b in zip(names, names[1:]):
    x, y, u, v, M = PIV(path + frame_a, path + frame_b,
        window_size=50,
        overlap=30,
        search_area_size=100)

    # Scaling:

```

```

# By default, all values are given in pixels/dt
# if pixel size is 3.367 and time interval (dt) is 16 min per frame,
# then factor = 3.367 x (60/16) = 3.367 x 3.75 = 12.63
u, v, M = scale2(u = u, v = v, M = M, factor = 10.527)
x = np.multiply(x, 0.7018)
y = np.multiply(y, 0.7018)

# Flipping v-components 180 degrees is required to obtain the correct vector orientation:
v = np.flipud(v)

# These operations reduce the number of arrows in the plot through averaging:
resized_x = scipy.ndimage.zoom(x, 0.6)
resized_y = scipy.ndimage.zoom(y, 0.6)
resized_u = scipy.ndimage.zoom(u, 0.6)
resized_v = scipy.ndimage.zoom(v, 0.6)
resized_M = scipy.ndimage.zoom(M, 0.6)

# Make the quiver plot:
fig, ax = plt.subplots(ncols=1, nrows=1)
im = plt.quiver(resized_x, resized_y, resized_u, resized_v, resized_M, clim=(0, 40), cmap="jet")
cb = fig.colorbar(im, label="Eyy (μm/h)")
cb.set_label("Speed (μm/h)")
ax.set_xlabel("X (μm)")
ax.set_ylabel("Y (μm)")
#plt.gca().set_aspect('equal', adjustable='box')
plt.savefig(path_out + "image" + str(k), dpi = 300)
print("Done with Image " + str(k))
k = k + 1

```

Appendix C: Complementary result of cell migration pattern of asynchronously growing cancer cells

Figure 17.D is cited in section 3.1.1 since the graph is most representative of the project. The cell lines used in this project was SW780, 5637 and T24. The figures are used as a reference for asynchronously (not starved) growing cancer cells. The graphs are showing average speed with standard deviation.

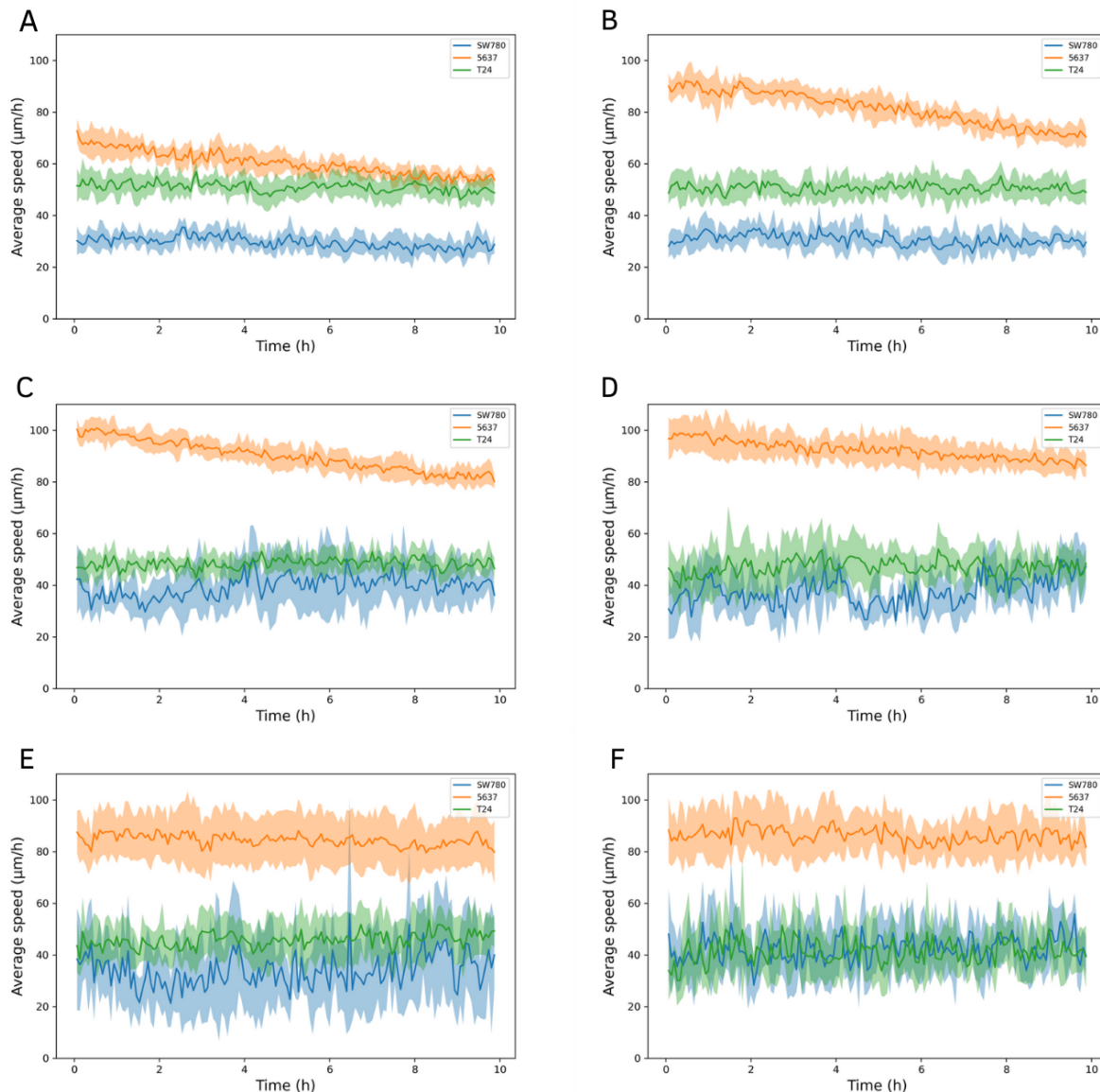


Figure 17: Cell movement in cell sheet of asynchronously growing cancer cells in various densities. The average migration speed of the cell lines SW780 (blue), 5637 (orange), and T24 (green) were monitored over a 10 hrs period on a high-content imaging ImageXpress Micro Confocal microscope. The darker color lines represent the mean velocity, while the lighter colored area is the standard deviation. The missing data point are due to irregular movements in the xy-stage of the microscope. Live cell imaging of cell sheets in wells with **A** 100,000 cells/well, **B** 50,000 cells/well, **C** 25,000 cells/well, **D** 12,500 cells/well, **E** 6,250 cells/well, and **F** 3,125 cells/well

Appendix D: Complementary result of cell migration pattern of quiescent and re-stimulated cancer cells

Figure 18.D and figure 19.D are cited in section 3.1.2 since the graphs gave the most representative results of the project. The cell lines used in this project was SW780, 5637 and T24. The cell sheet in figure 18 were exposed to serum deprivation to establish quiescent cell state, and in figure 19 the cells were re-stimulated with FBS after starvation. The graphs are showing average speed with standard deviation.

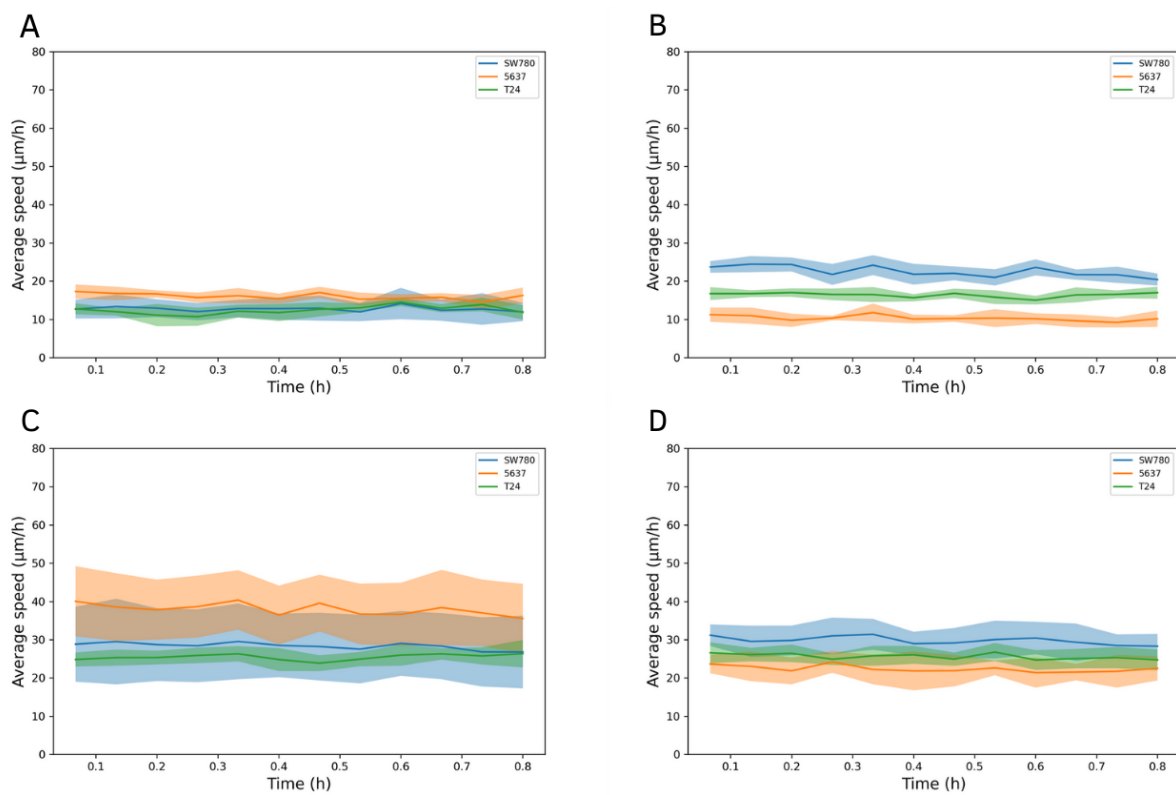


Figure 18: Cell movement in cell sheet of starved cancer cells in various densities. The average migration speed of the cell lines SW780 (blue), 5637 (orange), and T24 (green) were monitored a 1 h period on a high-content imaging ImageXpress Micro Confocal microscope. The darker color lines represent the mean velocity, while the lighter colored area is the standard deviation. Live cell imaging of cell sheets in wells with **A** 100.000 cells/well, **B** 50.000 cells/well, **C** 25.000 cells/well, and **D** 12.500 cells/well.

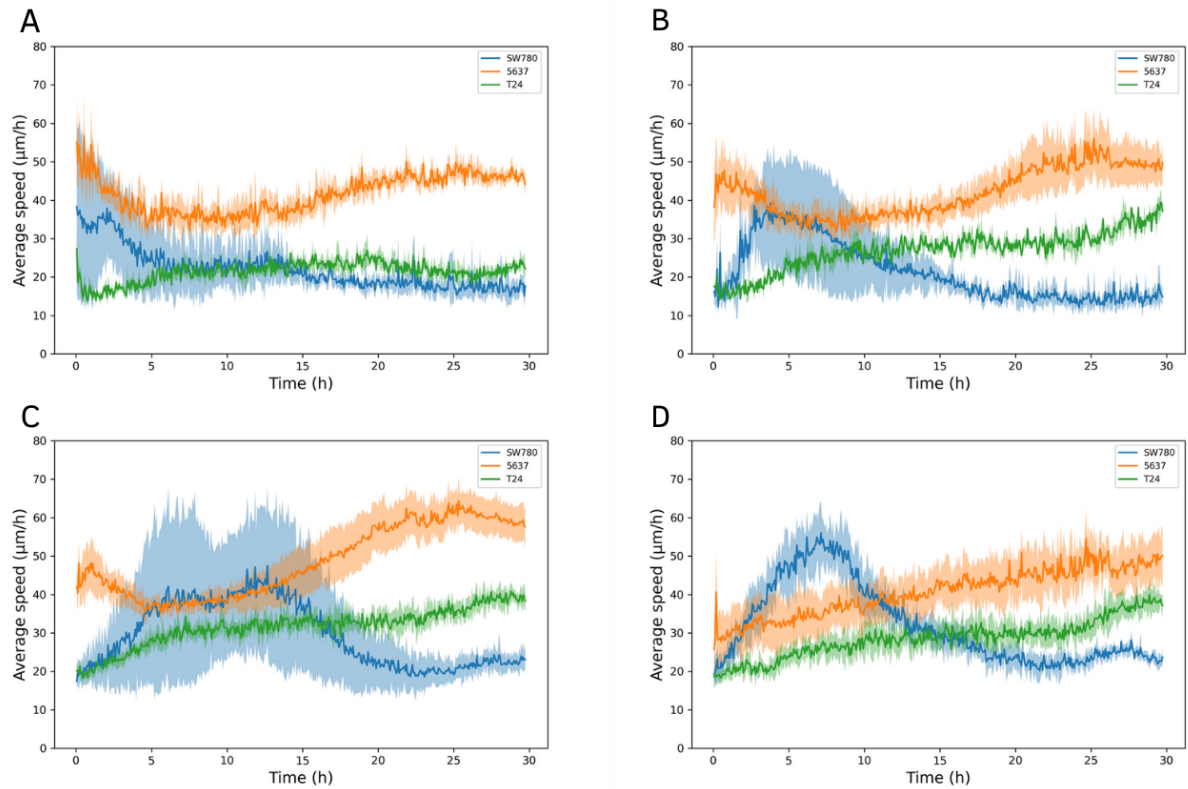


Figure 19: Cell movement in cell sheet of re-stimulated cancer cells in various densities. The average migration speed of the cell lines SW780 (blue), 5637 (orange), and T24 (green) were monitored a 30 hrs period on a high-content imaging ImageXpress Micro Confocal microscope. The darker color lines represent the mean velocity, while the lighter colored area is the standard deviation. Live cell imaging of cell sheets in wells with **A** 100.000 cells/well, **B** 50.000 cells/well, **C** 25.000 cells/well, and **D** 12.500 cells/well.

Appendix E: Information about the cell lines used in this project

Table 2: Information about the different cancer cell lines.

NAME	GENDER	AGE	ETHNICITY	DISEASE	SUBCULTIV. RATIO/MED. RENEW.	GROWTH MED.
T24	Female	81	Caucasian	TCC, high grade invasive (grade III)	1:3-1:8/2-3 times per week	McCoy's 5a M M + 10% FBS
SW780	Female	80	Caucasian	TCC, grade I	1:4-1:8/2-3 times per week	DMEM + 10% FBS
5637	Male	68	Caucasian	TCC, grade 2	1:4-1:8/2-3 times per week	RPMI-1640 + 10% FBS

T24: Doubling time: 19 hours (PubMed=4133950 (Bubenik, 1973)); 21 hours (PubMed=3708594 (Masters, 1986)); ~48 hours(DSMZ); ~1 day (lot 02052018) (JCRB).

SW780: Doubling time: 38 hours.

5637: Doubling time: 23 hours (PubMed=26055179 (Vallo, 2015)); ~24 hours (DSMZ).